UNIVERSITY OF OKLAHOMA

GRADUATE COLLEGE

SUBSEASONAL WINTER WEATHER PREDICTABILITY ASSOCIATED WITH SINGLE VS. MULTIPLE WAVE PULSE EVENTS AND THEIR IMPACT ON THE ARCTIC STRATOSPHERIC POLAR VORTEX

A THESIS

SUBMITTED TO THE GRADUATE FACULTY

in partial fulfillment of the requirements for the

Degree of

MASTER OF SCIENCE IN METEOROLOGY

By

JACOB OHNSTAD
Norman, Oklahoma
2020

SUBSEASONAL WINTER WEATHER PREDICTABILITY ASSOCIATED WITH SINGLE VS. MULTIPLE WAVE PULSE EVENTS AND THEIR IMPACT ON THE ARCTIC STRATOSPHERIC POLAR VORTEX

A THESIS APPROVED FOR THE
SCHOOL OF METEOROLOGY

BY THE COMMITTEE CONSISTING OF

Dr. Jason C. Furtado, Chair

Dr. Naoko Sakaeda

Dr. Elinor R. Martin

Acknowledgments

This work could not be completed alone. The author would like to thank the thesis committee for their time and willingness to give ideas and support through this process. I would like to thank Dr. Jason Furtado for his assistance with the research, his mentorship, and his time spent editing. Furthermore, I would like to thank my family and friends for their support. The author thanks Judah Cohen and Matthew Barlow for their collaboration on this research. This work is supported by the National Science Foundation (NSF) grant AGS-16S7905.

Table of Contents

Acknowledgments **iv**

List of Tables **vi**

List of Figures **vii**

Abstract **xi**

1 Introduction **1**
1.1 The S2S Timescale: Background and Previous Literature 1
1.2 The Stratospheric Polar Vortex and its Disturbances 4
1.3 Thesis Goals and Hypotheses 11

2 Data and Methods **13**
2.1 Data 13
2.2 Methods 14
2.3 Compositing Methods 18

3 Characteristics of Single and Multiple Wave Pulse Events **21**
3.1 Single vs. Multiple Pulses in Reanalysis 21
3.1.1 Spatial Geopotential Height and Heat Flux Patterns 21
3.1.2 Impact on the Stratospheric Polar Vortex 25
3.1.3 Vertical Characteristics and Evolution 29
3.1.4 Discussion of Reanalysis Results 30

4 Single vs. Multiple Pulses in S2S Models and Origin of Wave Pulses **37**
4.1 Single vs. Multiple Pulses in S2S Hindcast Models 37
4.1.1 Tropospheric Spatial Geopotential Height Patterns 37
4.1.2 Stratospheric Spatial Heat Flux Pattern 40
4.1.3 Impact on the Stratospheric Polar Vortex 40
4.2 Origin of Wave Pulse Events 42
4.2.1 Discussion of S2S Model Results and Pulse Origin 46

5 Summary and Conclusions **48**

Reference List **51**

List of Tables

2.1 Information for each model dataset in the model mean as well as the number of events that each model produced. 14

4.1 Single pulse event region information for each dataset. N-value is total # of events found in each dataset. Percent based on number of events inside each region divided by the N-value in each dataset. 44

4.2 Same as Table 4.1 but for the first pulse of multiple pulse events. . . 45

4.3 Same as Table 4.1 but for the second pulse of multiple pulse events. Last row indicates how often 1^{st} and 2^{nd} pulse occur in the same region. 46

List of Figures

1.1 A schematic representation of many of the atmospheric phenomena and numerical modeling considerations needed to make accurate forecasts in the subseasonal-to-seasonal time scale. Adapted from Lang et al. (2020). 3

1.2 Northern Hemisphere wintertime (December-February) 100 hPa climatological (1981-2010) heat flux. 9

1.3 Extended winter season standardized area-averaged (40°N-80°N) vertical wave activity flux for (top) 2012-13 and (bottom) 2013-14. . . . 10

2.1 Time series of 100 hPa area-averaged heat flux (K ms^{-1}) from 40°N-80°N for a multiple pulse event (blue), a single pulse event (purple), and an event where no pulses were identified (red). Grey line indicates the 75^{th} percentile used in the first set of criteria to find an event day. Black line indicates 85^{th} percentile used in the second set of criteria to identify the peaks. Pink circles indicate the point of a peak given criteria. 18

2.2 Reanalysis number of heat flux events per winter season for 81 single pulse events (blue) and 23 multiple pulse events (purple). Black stars indicated year or winter season in which a major SSW event occurred. 19

3.1 Lag composites of 500 hPa geopotential height anomalies (m) for (top) 81 single pulse events and (bottom) 23 multiple pulse events from Day -5 to Day +10 and Day 0 being the start day of the events. Statistical significance ($p < 0.05$) done using a two-sided Student t-test. Statistical significance indicated by the gold contour. 23

3.2 As in Fig. 3.1 but for 100 hPa heat flux anomalies (K ms^{-}1). Statistical significance ($p < 0.05$) done using a two-sided Student t-test indicated by the light blue contour. 25

3.3 As in Fig. 3.1 but for 10 hPa geopotential height anomalies (m). Statistical significance ($p < 0.05$) done using a two-sided Student t-test indicated by the gold contour. 27

3.4 Time series of 10 hPa zonal wind from 60°N for (a) single pulse events, (b) multiple pulse events, and the (c) difference between them. (a,b) Grey shading indicates +/- one standard deviation around the event mean indicated by the solid black line. Vertical blue line indicated the identified start date of events and horizontal red line indicates the line of the wind being zero. Events that fall below the red line indicate a major SSW event occurred. Positive U-Wind values indicate a westerly wind and negative values indicate an easterly wind. (c) The difference between the mean line in a and b. The line is red when the difference in the two means is statistically significant using a two-sided Student t-test at the 95% confidence level. 28

3.5 Lag composite of area-averaged (left) standardized heat flux (40°N-80°N) and (right) standardized GPH (60°N- 90°N) from -60 to +60 days as a function of pressure (hPa). (a,b) Composites of 81 singe pulse events. (c,d) Composites of 23 multiple pulse events. Day 0 represents the start date of the event (see text). Statistical significance done using a two-sided Student t-test at the 95% confidence interval indicated by the black contour. 30

3.6 Cumulative area-averaged heat flux (K ms^{-1}) for each reanalysis event. Purple dots indicate single pulse events and blue dots indicate multiple pulse events. Lines of those respective colors indicate events mean. Triangles indicate major SSW events that are associated with a particular single (red) or multiple (green) pulse event. 33

3.7 Lag composite of surface temperature anomalies (°C) for 81 single pulse events from Day -5 to Day +30 and Day 0 being the start day of the events. Statistical significance ($p < 0.05$) done using a two-sided Student t-test. Statistical significance indicated by the brown contour. 35

3.8 As in Fig. 3.7 but for 23 multiple pulse events. 36

4.1 As in Fig. 3.1 but multi-model mean. Statistical significance for the multi-model mean found by 5 out of 6 models having same sign anomaly. Statistical significance indicated by the gold contour. Note that values on the colorbar are half of that displayed in Fig. 3.1. . . . 39

4.2 As in Fig. 3.2 but for the multi-model mean. Statistical significance for the multi-model mean found by 5 out of 6 models having same sign anomaly. Statistical significance indicated by the light blue contour. Note that values on the colorbar are half of that displayed in Fig. 3.2. 41

4.3 As in Fig. 3.3 but for multi-model mean. Statistical significance for the multi-model mean found by 5 out of 6 models having same sign anomaly. Statistical significance indicated by the gold contour. 42

4.4 Origin of wave pulse events for single (left) and multiple (right) pulse events. Solid lines outline the individual regions of Europe (green), Siberia (red), North Pacific (blue), and North America (purple). Individual dots indicate the location of the maximum heat flux value inside the region found to contain the wave pulse event (maximum area-averaged heat flux). Red dots indicate the first pulse maximum (or only pulse for single pulse events) and blue dots indicate the second pulse maximum. 43

Abstract

Variability in the Arctic stratospheric polar vortex can lead to extreme winter weather across the Northern Hemisphere, which can have large socioeconomic impacts. Dynamically, increased vertical wave activity from the troposphere into the polar stratosphere fluxes anomalous heat towards the pole, resulting in the warming and weakening of the stratospheric polar vortex. Characteristics of these vertical wave driving events are not well understood as they can vary in strength, duration, and location. This research addresses the knowledge gap associated with vertical wave driving characteristics and the impact they have on the stratospheric polar vortex. Here we compare the impacts of single versus multiple vertically propagating wave events entering the polar stratosphere in both ERA-Interim and hindcasts of operational subseasonal models in the Subseasonal-to-Seasonal (S2S) Prediction Project Database. Tropospheric height patterns that occur on the start day of single and multiple pulse events include anomalous ridging over Northern Eurasia and the North Atlantic as well as an anomalous trough or zonal trough-ridge pattern over the North Pacific. These anomalous patterns are co-located with large meridional heat flux anomalies during the events. Single pulse events have less persistent tropospheric features and are found to be relatively short-lived and weaker compared to multiple pulse events. As a result, the vortex is much weaker following multiple pulse events than single pulse events. The significant stratospheric anomalies that occur with these events more readily downward propagate into the troposphere following multiple pulse events versus single pulse events. S2S models capture well the spatial patterns of single and multiple pulse events on the start day of the event, but struggle to produce stationary features at later lags, such as blocking highs, which are important for producing multiple pulse events. In both reanalysis and S2S models, the North Pacific, Europe, and Siberia are the regions favored for the origin of the pulses. Analyzing these wave pulse events will shed light on the different characteristics which

produce a wave pulse event and the impacts these events have on the stratospheric polar vortex which may subsequently improve subseasonal winter weather forecasts.

Chapter 1

Introduction

Extreme winter weather is often dominated by severe cold-air outbreaks and strong extratropical cyclones which have large socioeconomic impacts. Among other teleconnection patterns, these extreme weather events are tied to variability in the stratospheric polar vortex (Kidston et al., 2015). Polar vortex variability is most often tied to a weakened polar vortex which results from waves propagating vertically from the troposphere into the polar stratosphere (e.g., Charney and Drazin, 1961; Edmon Jr et al., 1980; Plumb, 1985; Polvani and Waugh, 2004). When the stratospheric polar vortex is perturbed, the associated anomalies often propagate downward into the troposphere days later, altering tropospheric jet streams and influencing surface weather patterns on time frames of weeks to months (e.g., Baldwin and Dunkerton, 1999, 2001; Thompson and Wallace, 2000; Polvani and Waugh, 2004). This time frame is known as the sub-seasonal to seasonal (S2S) timescale (i.e., the period roughly spanning two weeks to three months; Brunet et al., 2010; National Academies of Sciences, Engineering and Medicine, 2016) The meteorological community particularly struggles with improving the predictability of extreme weather events (including polar vortex disruptions and cold-air outbreaks) on the S2S timescale (e.g., Karpechko et al., 2018; Lee et al., 2019b). Understanding and analyzing the events that weaken the polar vortex can help improve the knowledge surrounding winter weather predictability associated with the stratospheric polar vortex.

1.1 The S2S Timescale: Background and Previous Literature

In recent decades, there has been increasing interest for forecasts, between the short (1-10 days) and the long term (3+ months), or the S2S timescale. The S2S

timescale is an important period to increase the skill of forecasts and weather related risks (e.g. drought, heat waves, cold air outbreaks, and precipitation) as it can provide important lead-time for socioeconomic risks. However, most forecast skill of S2S forecasts is lacking compared to other forecasts. Current capabilities of the short term numerical models do not extend skill past roughly 10 days, and most seasonal models only provide skill beyond 3 months as they do not consider the dynamics of S2S mechanisms or important modes of variability which affect weather on shorter timescales. For this reason, the S2S time frame particularly lacks forecast skill, increasing its priority for research (Vitart and Robertson, 2018). Recently, research projects have addressed this knowledge gap. For example, the S2S Prediction Project aims to improve forecast skill and fundamental understanding of the sources of S2S predictability, and promote its use by operational centers the application communities (Robertson et al., 2015; Vitart et al., 2017; Vitart and Robertson, 2018). An extension of this project also aims to "identify common successes and shortcomings in the model simulation and prediction of sources of subseasonal to seasonal predictability" (Vitart et al., 2017). Several patterns of variability have to be considered when making S2S forecasts, some of which include variability in stratospheric polar vortex, the Madden Julian Oscillation (MJO), the North Atlantic Oscillation (NAO), sea ice, sea surface temperature anomalies, and changes in land surface (Fig. 1.1). Lang et al. (2020) describes how these modes of variability can interact to create skill in S2S forecasts. For example, lack of sea ice in the Barents-Kara Sea increases surface temperatures, which could lead to a blocking ridge over Eurasia. Blocks increase vertically propagating waves which impact the stratospheric polar vortex and can lead to tropospheric jet changes and cold air outbreaks across portions of the Northern Hemisphere as demonstrated in Figure 1.1. Cai et al. (2016) notes a similar process of increased vertical wave activity disrupting the polar vortex which can lead to the prediction of cold extremes one month in advance using S2S models.

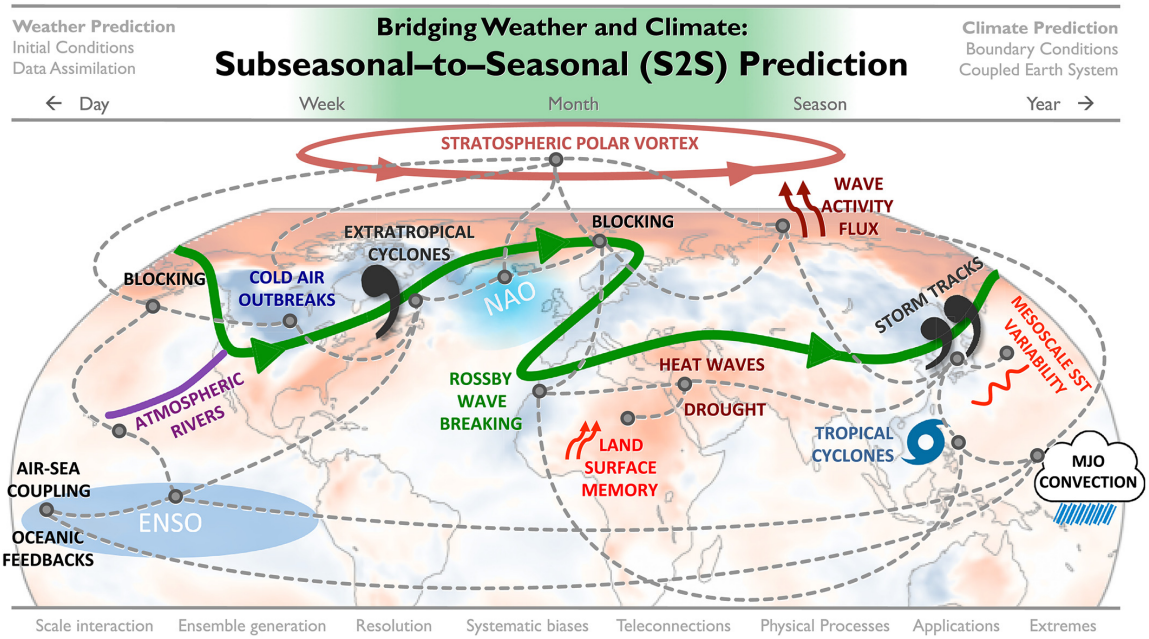

Figure 1.1: A schematic representation of many of the atmospheric phenomena and numerical modeling considerations needed to make accurate forecasts in the subseasonal-to-seasonal time scale. Adapted from Lang et al. (2020).

While increased interest into the S2S time frame is recent, several meteorological/climate features have been investigated on their role in S2S predictability. For example, Lim et al. (2019) investigated the predictability of Australian heat waves and drought on the S2S timescale following a weakened Southern Hemisphere stratospheric polar vortex. Similarly, Karpechko et al. (2018) explored predictability of a weakened polar vortex in S2S models and associated wintertime weather impacts across the Northern Hemisphere. Some other atmospheric modes analyzed at the S2S timescale include: MJO prediction (e.g., Lim et al., 2018; Tseng et al., 2018), the MJO and its interactions with the stratospheric polar vortex to shape S2S weather regimes (e.g., Garfinkel et al., 2012; Green and Furtado, 2019), the Quasi-biennial Oscillation (QBO) and MJO prediction (e.g., Lim et al., 2019; Kim et al., 2019), extreme rainfall (e.g., White et al., 2015; Jennrich et al., 2020), and the persistence of extreme winter weather regimes across the Northern Hemisphere (e.g., Cassou, 2008;

Lee et al., 2019a; Domeisen et al., 2020a). A few of these studies focus on the predictive skill associated with stratospheric phenomena, particularly the stratospheric polar vortex. When discussing the stratospheric polar vortex, understanding the state of the vortex (i.e., whether it is in a strong or weak state) can be important for skillful S2S predictions (e.g., Jucker and Reichler, 2018; Karpechko et al., 2018; Lee et al., 2019b; Domeisen et al., 2019; Butler et al., 2019; Domeisen et al., 2020b).

Yet, there are several occurrences of S2S extreme events accompanied with major socioeconomic impacts. Since 1980 there have been 17 billion-dollar disasters due to winter weather extremes across the United States, 9 of which are related to cold air outbreaks causing large scale agricultural damage (NOAA National Centres for Environmental Information, 2020). Kretschmer et al. (2018) shows that cold air outbreaks have increased in persistence over the last few decades over portions of the Northern Hemisphere, such as Siberia, due to a more persistent weak polar vortex. A weakened polar vortex along with amplified modes in the North Pacific played a role in the record cold winter of 2013-14 across the eastern United states (Marinaro et al., 2015; Baxter and Nigam, 2015). A more complete understanding of these events may help forecasters predict them and public officials prepare for the impacts of a weakened polar vortex.

1.2 The Stratospheric Polar Vortex and its Disturbances

Research on the stratospheric polar vortex has been increasing over the past several decades due to the further understanding that the stratosphere and the troposphere are not exclusive from one another and often interact, especially during the winter months (Baldwin and Dunkerton, 1999, 2001; Cohen et al., 2007). Charney and Drazin (1961) showed the planetary-scale waves (mainly wave-1 and wave-2) can propagate beyond the troposphere and into the stratosphere given the stratospheric

vortex had westerly winds and that they were not too strong. Matsuno (1970) displayed that planetary waves 1 and 2 are often amplified in the Northern Hemisphere during the winter months due to the increase in meridional temperature gradient across the midlatitudes, which is reinforced by large continental land masses and mountain ranges. In the Southern Hemisphere, waves 3, 4, and 5 are much more common, while waves 1 and 2 are rare due to the lack of land in the middle and high latitudes. Furthermore, Edmon Jr et al. (1980) created a diagnostic tool to visualize wave propagation–the Eliassan-Palm (EP) Flux. The EP Flux cross-sections tell us where there is divergence or convergence of waves both in latitude and altitude. Knowledge of the convergence of waves allows us to know if there will be an impact on the stratospheric polar vortex. Plumb (1985) expanded on this study by creating a wave flux which had a spatial extent in order to locate where waves that enter the stratosphere originate across the Northern Hemisphere. Plumb (1985) showed that the vertical component of the wave activity flux (WAF) or Plumb flux, from the troposphere into the polar stratosphere, fluxes anomalous heat towards the pole, resulting in the warming and weakening of the stratospheric polar vortex (e.g., Charney and Drazin, 1961; Edmon Jr et al., 1980; Plumb, 1985; Chen and Robinson, 1992; Polvani and Waugh, 2004).

Traditionally, weak vortex events have been defined two ways. The most extreme polar vortex weakenings are called major sudden stratospheric warming (SSW) events, which occur when the temperatures at the poles rise tens of degrees Celsius in the matter of a few days and the winds in the polar night jet make a complete reversal to easterly winds (e.g., Christiansen, 2001; Limpasuvan et al., 2004; Karpechko et al., 2018). Major SSW events are divided into two categories based on the weakening pattern of the polar vortex. The vortex can either be displaced off the pole (vortex displacement events) or split into two distinct vortices (vortex splitting events). Vortex displacements and vortex splits are known to be predominantly associated with

vertically propagating waves of wavenumber 1 and 2, respectively (Andrews et al., 1987). The second type of weak vortex events are minor SSW events, where the polar vortex is still disrupted but not to the same extent as a major SSW. Minor SSWs both weaken the winds and warm the polar vortex, but the vortex does not split or get displaced off of the pole. The vortex often gets distorted or stretched instead. Kretschmer et al. (2018) showed, through cluster analysis, that minor SSWs occur with much greater frequency and can still have downward propagating impacts. Both minor and major SSW events can result in extreme winter weather regimes across portions of the Northern Hemisphere (Karpechko et al., 2017; Kretschmer et al., 2018).

Multiple different land-atmosphere interactions that can take place to cause the polar vortex to weaken, all of which include the precursor of anomalous vertical wave activity fluxed from the troposphere into the stratosphere. Atmospheric waves converge and break in the stratosphere displacing heat which warms and weakens the polar vortex (Edmon Jr et al., 1980; Plumb, 1985; Kidston et al., 2015). Waves break as their amplitude reaches a critical level in the stratosphere aided by the vertical shear of the polar vortex (McIntyre and Palmer, 1984). As mentioned previously, planetary waves 1 and 2 have the largest contribution to vertical wave propagation and meridional transport of heat into the stratosphere in both hemispheres leading to the disruption of the polar vortex (Matsuno, 1970, 1971; Limpasuvan et al., 2004). Waves 1 and 2 are the only waves able to propagate beyond the troposphere as the stratosphere is to stable for smaller atmospheric waves to propagate into (Charney and Drazin, 1961). The polar vortex is often too strong for these smaller waves (3+) to have a large enough impact to weaken the winds or shears the wave off before it can reach the middle and upper stratosphere (Charney and Drazin, 1961). Recently, studies identified particular regions across the Northern Hemisphere responsible for

increased areas of wave activity preceding SSW events, specifically over central Eurasia, the North Pacific, and the North Atlantic which can be seen in the climatological heat flux (Fig. 1.2; Cohen and Jones, 2011; Karpechko et al., 2018; Peings, 2019). There exists certain boundary conditions within these regions that favor or amplify planetary waves. Some studies suggests that anomalously high snowfall coverage over portions of Eurasia and/or lack of sea ice in the Barents-Kara Sea early in the winter result in sea level pressure changes across the Northern Hemisphere, favoring enhanced wave propagation (e.g., Jaiser et al., 2013; Cohen et al., 2014; Kim et al., 2014; Zhang et al., 2018). Most studies note the development of a Ural High preceding weak polar vortex events which amplifies the background stationary wave field and results in increased vertical wave activity in eastern Eurasia and the North Pacific on either side of the ridge (e.g., Cohen and Jones, 2011; Karpechko et al., 2018; Kretschmer et al., 2018; Peings, 2019). Lee et al. (2019b) also showed that a Rossby wave breaking event in combination with the intensification of the Ural high likely triggered the major SSW event in 2019. A blocking pattern, especially when the ridge is located over the Ural mountains, is known to amplify planetary waves which flux more wave energy into the stratosphere leading to a polar vortex disruption (Attard and Lang, 2019; Peings, 2019).

Additionally, following a disruption of the polar vortex, the stratosphere also influences tropospheric weather patterns (e.g., Haynes et al., 1991; Baldwin and Dunkerton, 1999, 2001). A weakened polar vortex creates positive height anomalies in the stratosphere as it warms due to a wave breaking event. These positive height anomalies propagate downward into the lower stratosphere as the vortex weakens. When the weakening of the vortex is substantial, the stratospheric anomalies that occur can be large enough to propagate downward into the troposphere and influence surface weather patterns on the S2S timescale (Kidston et al., 2015; Baldwin and Dunkerton, 2001; Karpechko et al., 2018; Lee et al., 2019b; Butler et al., 2019; Lang et al.,

2020). The tropospheric weather changes happen as a result of the troposphere and stratosphere becoming dynamically coupled during the weakening process of the polar vortex (Cohen et al., 2007; Kidston et al., 2015). For example, the Northern Annular Mode (NAM; Thompson and Wallace, 2000) and the NAO (Barnston and Livezey, 1987) shift toward the negative phase which have been shown to force large areas of cold temperature anomalies across the Northern Hemisphere for several weeks (e.g., eastern United States and Siberia; Baldwin and Dunkerton, 2001; Thompson and Wallace, 2001; Domeisen et al., 2015; Karpechko et al., 2018; Domeisen, 2019). SSW events also influence changes in sea ice extent in the Arctic due to circulation changes and warmer temperatures (Smith et al., 2018). However, not all weak vortex events have anomalies that propagate into the troposphere (Karpechko et al., 2017; Rao et al., 2020). These non-downward propagating events are accompanied with much smaller wave breaking events and a brief warming and weakening of the vortex (Karpechko et al., 2017, 2018; Domeisen et al., 2020b; Rao et al., 2020). Nevertheless, the knowledge surrounding the vertical propagation of planetary waves gave rise to the investigation of tropospheric mechanisms that amplify these waves, their impact on the stratospheric polar vortex, and the subsequent troposphere-stratosphere coupling.

Despite knowing this information about the polar vortex and its characteristics, models still struggle with being able to predict stratospheric disruptions more than 10-15 days in the future (Karpechko et al., 2018; Domeisen et al., 2020b). Past research has shown that models tend to underpredict the intensity of vertically propagating waves more than a few days prior to when they occur, therefore underestimating their impacts on the stratospheric polar vortex and making it hard to predict SSWs (Karpechko et al., 2018; Lee et al., 2019b). Oftentimes, models have insufficient stratospheric resolution which result in mediocre representation of the vertically propagating waves (e.g., Karpechko et al., 2018). Poor forecasting of these wave breaking

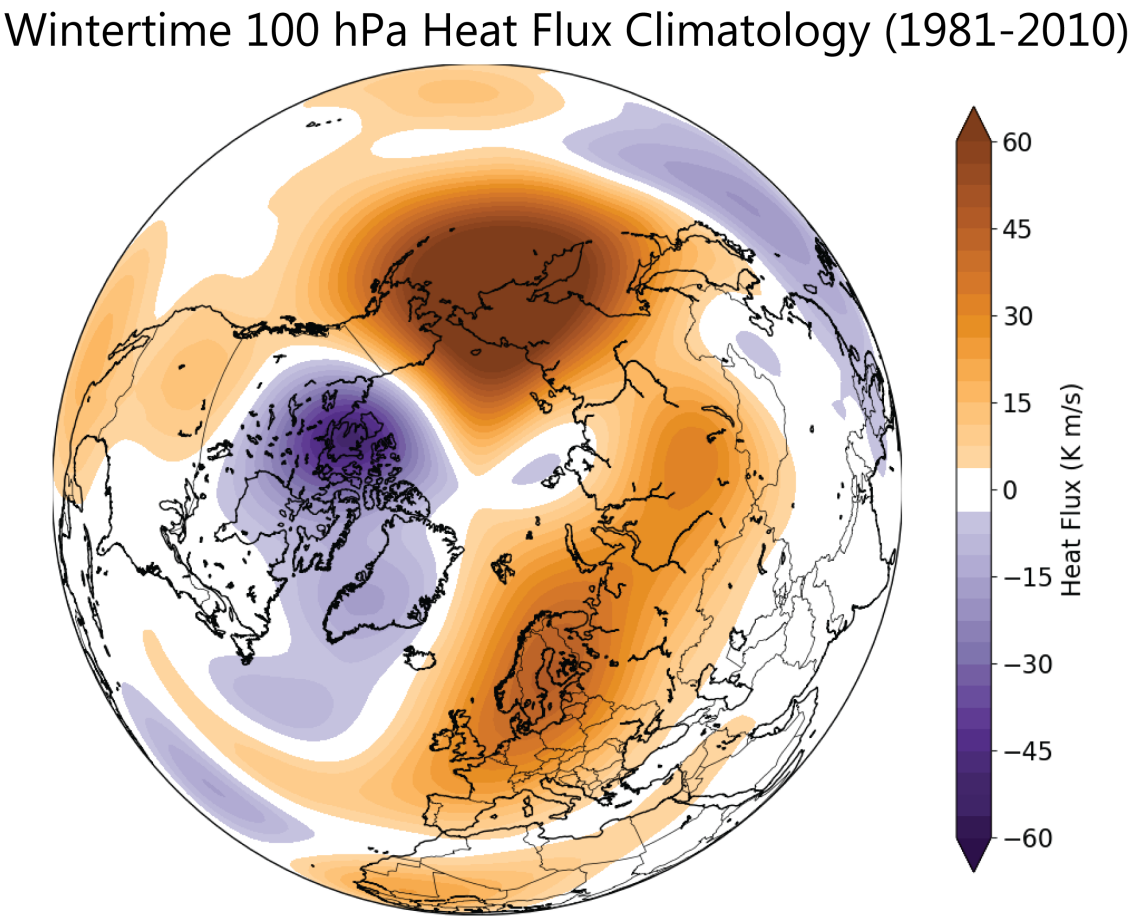

Figure 1.2: Northern Hemisphere wintertime (December-February) 100 hPa climatological (1981-2010) heat flux.

events makes it difficult to add skill to S2S forecasts before these events occur. Thus, having to wait until after the event occurs to see how the stratospheric polar vortex impacts will propagate down to the surface. Understanding the precursors of a blocking pattern as a result of the Ural high, how long the block lasts, and how much they amplify the vertical wave activity flux in places such as the North Pacific and North Atlantic can result in considerable differences in how the stratospheric polar vortex is perturbed. Models that represent these precursors accurately could help produce better seasonal forecasts for the winter months across the Northern Hemisphere.

Still, each pulse of wave activity flux into the stratosphere is different. Little research has been done to investigate the difference in duration, intensity, and location

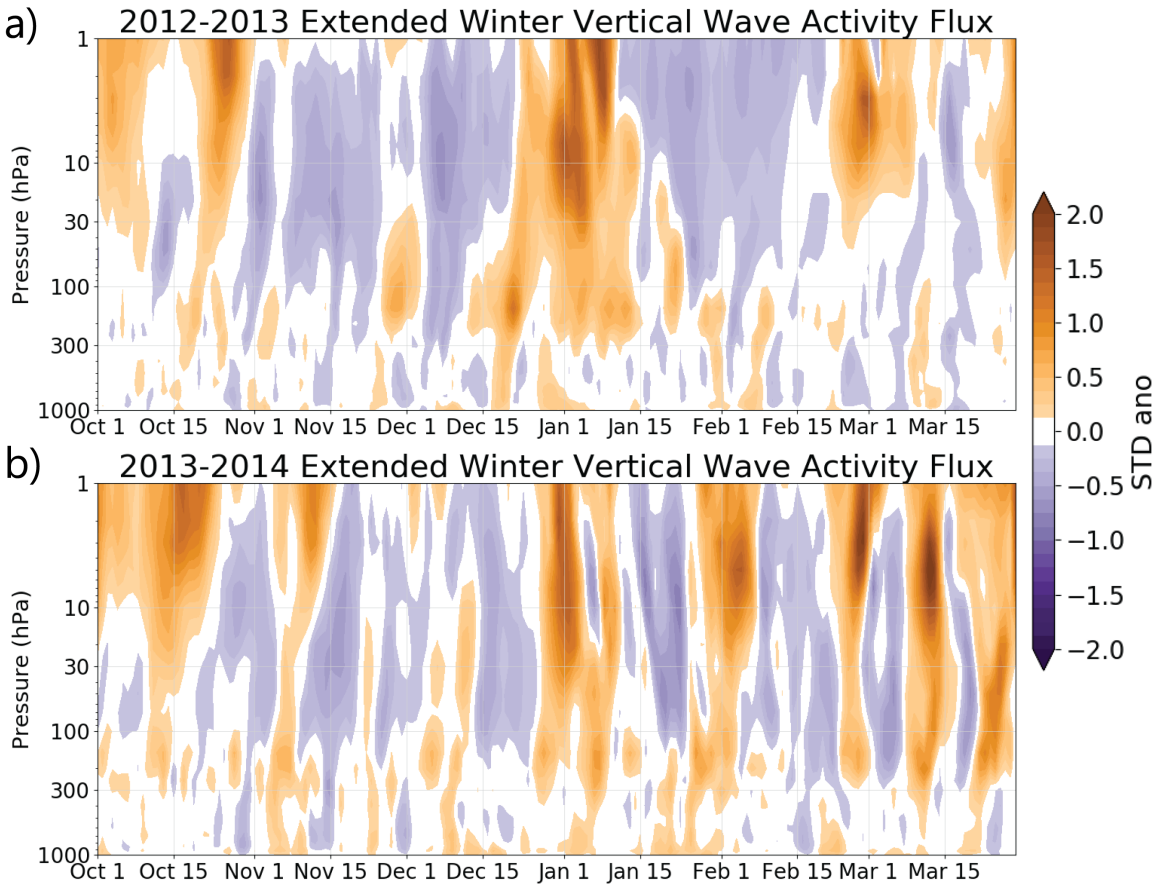

Figure 1.3: Extended winter season standardized area-averaged (40°N-80°N) vertical wave activity flux for (top) 2012-13 and (bottom) 2013-14.

of individual wave pulse events and their impact on the stratospheric polar vortex. Motivation for these differences can be seen during the winters of 2012-13 and the following winter of 2013-14 (Fig. 1.3). During the winter of 2012-13 there was one large wave-breaking event in the stratosphere. The wave-breaking event is characterized by the high amplitude standardized wave flux between 30 and 1 hPa in late December 2012 that caused a major SSW event to occur in early January 2013 (Fig. 1.3a). The next winter season there were multiple wave pulse events in the stratosphere that occurred over the period of late December 2013 through the end of March 2014 which resulted in a minor SSW event (Fig. 1.3b). The 2013-14 winter was also the coldest winter across the eastern United States in recent history (Marinaro et al., 2015).

Therefore, differences in the number of wave events could result in different impacts on the polar vortex. Analyzing these wave pulse events, including their fundamental characteristics and statistics, may shed light on the different impacts these events have on the stratospheric polar vortex and subsequently improve subseasonal winter weather forecasts.

1.3 Thesis Goals and Hypotheses

Given the increased interest and need for understanding the stratospheric polar vortex and associated predictability in the S2S framework, this thesis addresses some of the gaps in understanding polar vortex disruptions. The key goal of this research is to enhance the understanding of the large-scale dynamics associated with vertically propagating waves and how different waves can cause a different impact on the stratosphere. More specifically, we compare the impacts and precursors of single versus multiple (i.e., a series of anomalously strong vertically propagating waves entering the polar stratosphere) wave events, such as those seen in the winters of 2012-13 and 2013-14. Additionally, ERA-Interim reanalysis data is compared to data from S2S hindcast models in the S2S Prediction Project Database (Vitart et al., 2017) to investigate how well long range models produce these events. Model-produced events also help to increase the sample size of our events and their outcomes. We hypothesize that both single and multiple vertically propagating wave events have varying impacts on the stratospheric polar vortex with multiple pulse events having both a greater magnitude and duration of impact. Furthermore, we hypothesize that the S2S models will produce similar results to that of reanalysis surrounding the events with the possibility of many more events within the model associated with increased sample size. Also, the spatial pattern (possible blocking pattern) between the events will look relatively similar but be longer lasting for multiple wave events providing a more conducive setup for more waves to propagate vertically. If we can further

understand what kind of impacts different waves have on the stratosphere then it is through projects such as this that the prediction and understanding of S2S events will improve.

The thesis is organized as follows. Data and methodology used for this study, including the event identification algorithm, are described in Chapter 2. Chapter 3 contains the results and discussion of the composite analysis for ERA-Interim wave pulse events, including both vertical and spatial characteristics of the pulses. S2S model event results as well as the location of the wave pulse events across the Northern Hemisphere along with a discussion of each is found in Chapter 4. Lastly, Chapter 5 provides a summary and conclusion of the findings.

Chapter 2

Data and Methods

2.1 Data

To first investigate wave pulse events, we use daily-mean ERA-Interim (Dee et al., 2011) reanalysis data from 1979-2019 which has a horizontal resolution of 1.5° x 1.5° and 23 vertical pressure levels including 12 in the stratosphere. We use variables such as geopotential height, air temperature, and the meridional and zonal winds to conduct our analysis. We compare the reanalysis results with daily-mean data from several S2S hindcast model datasets which we use to form a multi-model mean. The S2S models are from the S2S Prediction Project Database which includes near-real-time ensemble forecasts and hindcasts up to 62 days in length and ranging from 1981-2016 from 9 centers (Vitart et al., 2017). Table 2.1 provides an overview of the models used in this study. Of the nine S2S datasets, six were used for further analysis, ISAC-CNR, JMA, and the ECCC are excluded here since they did not produce any multiple pulse events. Horizontal resolution for all models except BOM is 1.5° x 1.5° (BOM lies on a 2.5° x 2.5° horizontal grid). BOM output is subsequently interpolated onto the same 1.5° x 1.5° grid by a cubic interpolation method to form the multi-model mean. All models output have 10 vertical pressure levels including 3 in the stratosphere (100, 50, and 10 hPa).

For this study, we use daily-mean data from each of the datasets. We restrict the analyses to the extended boreal cold season (October-March), as this is the active period for the Northern Hemisphere polar vortex. For measuring the vertical propagation of waves, we use an averaged zonal-mean eddy heat flux, denoted as $[v^*T^*]$ (where v indicates the meridional component of the wind and T indicates air temperature, the star notation indicates a departure from the zonal mean and the brackets

Table 2.1: Information for each model dataset in the model mean as well as the number of events that each model produced.

Model / Model Info	ECMWF	UKMO	CMA	NCEP	KMA	BOM
# of Ensemble Members	10	2	3	3	2	32
Length (days)	47	61	61	45	61	62
Hindcast Period	1996-2014	1993-2015	1994-2014	1999-2010	1991-2010	1981-2013
Initializations	Every 7 days	Every 8 days	Every day	Every day	Every 8 days	Every 5 days
# of Event (single/multiple)	1115 / 6	413 / 9	4744 / 87	1280 / 11	372 / 12	14090 / 333
Modeling Center	European Centre for Medium-Range Weather Forecasts	United Kingdom Met Office	China Meteorological Administration	National Centers for Environmental Prediction	Korea Meteorological Administration	Australian Bureau of Meteorology

indicate a zonally averaged quantity) which is proportional to the vertical component of the Plumb wave activity flux (i.e. WAFz, Plumb, 1985). Using WAFz does not change the results but calculating meridional heat flux is more efficient and consistent across datasets as the S2S models do not have enough vertical resolution to do the vertical derivatives needed for the WAFz calculations. Reanalysis anomaly fields are calculated by removing the 1981-2010 daily climatological mean. Model means are taken across all files within a given model with the same initialization date as the one where an event is located. S2S anomaly fields are then found by removing the mean from each event day within that specific event.

2.2 Methods

We use two phases of criteria to define single and multiple wave pulse events. The first set of criteria identifies days where there is wave driving from the troposphere to the stratosphere. The second set looks at each of these wave driving events in more detail and identifies their robust features. We do this further investigation to identify the peaks in wave activity throughout the wave pulse events as they are usually different in structure, duration, and intensity from one another. Understanding these

characteristics may give more insight into the impacts they have on the polar vortex and eventually changes in surface weather on the S2S timescale. Once a list of wave pulse events is identified, we characterize each wave pulse event into two subcategories. These categories separate the heat flux events into single and multiple wave pulse events.

First, we examine the meridional heat flux at two pressure levels in the atmosphere: 500 and 100 hPa. These heights are chosen to represent the middle troposphere and lower stratosphere, respectively. The heat flux field is subsequently area-averaged between 40°N – 80°N. We define a wave pulse event day when the daily-mean area-averaged heat flux value is positive at the 500 hPa pressure level (roughly $> 52^{th}$ percentile) and reaches or exceeds the 75^{th} percentile of the given distribution at the 100 hPa pressure level. The positive 500 hPa heat flux value changes between the 52^{nd} and 53^{rd} percentile depending on the dataset. As such, events represent coherent positive vertical wave propagation, on average, from the troposphere into the lower stratosphere. These values were chosen to allow for a large sample size of events (so as to not just focus on "extreme" wave propagation events) for analysis. Event criteria focuses more on the wave events reaching the lower stratosphere which are likely responsible for the changes in the stratospheric polar vortex.

Event days are strung together when there is no more than 6 days of separation between the next day above the percentiles. Event days separated by 7 or more days are considered an "independent" or a separate event. 7 days was subjectively chosen as the separating time frame between two event days as atmospheric characteristic change dramatically over a 7 day period and event days are likely no longer connected. Any event that is shorter than 3 days long is removed from the event list as the identification of a peak requires 2 side points and a middle point to ensure a substantial wave pulse occurred. Start and end dates for each event were determined

as the first and last day in each of the discovered events. These criteria yield 159 events within the ERA-Interim dataset.

Furthermore, once we determine start and end dates of the events, time series for each plot were created to analyze the evolution of each heat flux event at 100 hPa (Fig. 2.1). Using the second set of criteria, we separate each event into single and multiple wave pulse events based on the number of peaks contained in each event time series. A peak is defined when:

1. The height of the peak surpasses the 85^{th} percentile for 100 hPa heat flux

2. The prominence of the peak, which determines how much a given point stands out from its surrounding points, must be at or greater than a value given by: 10% of the heat flux 95^{th}-percentile value of a given dataset distribution (roughly 1.5 Kms^{-1} for all datasets)

3. In the case of more than one peak per event, peaks must be between 3-7 days apart

In the case that two peaks are greater than 7 days apart that event is considered two separate wave pulse events. These criteria produced 23 multiple pulse and 81 single pulse events within the ERA-Interim dataset. 55 events from the initial event list did not contain peaks that met these criteria and thus were discarded. Variations in these criteria yield 35-91 single pulse events and 11-23 multiple pulse events. For example, increasing the number of days between peaks to 3-10 days results in 3 more multiple pulse events and 9 less single pulse events. Doubling the prominence value results in 2 less multiple pulse events and 15 less single pulse events, and changing the height criteria to the 90^{th}-percentile results in 6 less multiple pulse events and 12 less single pulse events.

We use the same criteria in the S2S models as in the reanalysis dataset with all thresholds relative to the specific dataset. One added criterion to the model events

was that a model event must occur after the first five days and before the last 10 days in the model run to ensure lag composite imagery could be produced as hindcasts range from only 45-62 days long (Table 2.1). Eliminating the beginning and end days in the hindcasts may also be seen as an independence measure as the same event cannot be captured day after day in a model if runs are initiated every day such as the NCEP and CMA models. We test each model hindcast, as well as each ensemble member, that occurs in the extended winter season for heat flux events. These criteria yield numerous single pulse events but a limited number of multiple pulse events (Table 2.1). Possible reasons for the differences in the number of events is discussed later in Chapter 4. We produce a multi-model mean of the events from the six models to compare model produced events to reanalysis events. We then assign the new start dates for each event to be the day of the first peak. Choosing a new start date was done to provide a common start date for each event as the day of the first peak does not always fall on the same given day of the defined events. The end of an event is defined by the last day that reaches the first set of criteria (i.e., the last day to meet or surpass the 500 hPa and 100 hPa heat flux percentiles).

As a verification mechanism that the wave pulse criteria capture significant events that impact the stratospheric polar vortex, we compared event dates with the dates of major SSW events found in the Sudden Stratospheric Warming Compendium in Butler et al. (2017). There are 25 major SSW events found in the ERA-Interim reanalysis dataset, and 24 of the 25 were found to be associated with these wave pulse events (i.e., wave pulse peak within $\sim$10 days of SSW date). The only event that was left out was the major SSW event that occurred in February 1979. As a result of these findings, we are confident that our method of finding wave pulse events is adequate for further analysis. All major SSW events as well as the number of ERA-Interim heat flux events per year are seen in Figure 2.2.

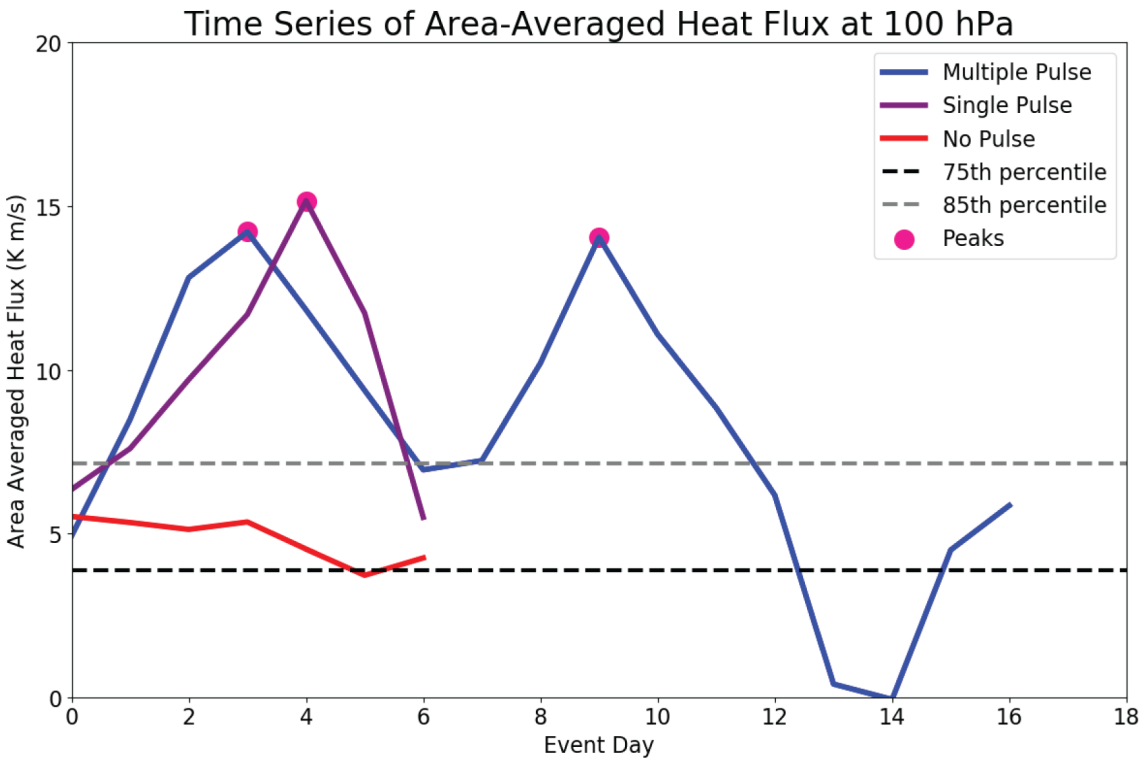

Figure 2.1: Time series of 100 hPa area-averaged heat flux (K ms^{-1}) from 40°N-80°N for a multiple pulse event (blue), a single pulse event (purple), and an event where no pulses were identified (red). Grey line indicates the 75^{th} percentile used in the first set of criteria to find an event day. Black line indicates 85^{th} percentile used in the second set of criteria to identify the peaks. Pink circles indicate the point of a peak given criteria.

2.3 Compositing Methods

With a list of single and multiple pulse events, composites of the ERA-Interim and model variables are then used to identify significantly anomalous patterns across the Northern Hemisphere. Two types of composites are used in this analysis. First, composited spatial plots of the Northern Hemisphere include 4 lags (-5, 0, +5, and +10 Days) to view the variables before, during, and after the events. Composites were made of both ERA-Interim and the multi-model mean for single and multiple pulse events. Secondly, composited plots of reanalysis area-averaged quantities are viewed in a time (-60 to +60 Days) by pressure (1000 hPa to 1 hPa) plot. These plots are used

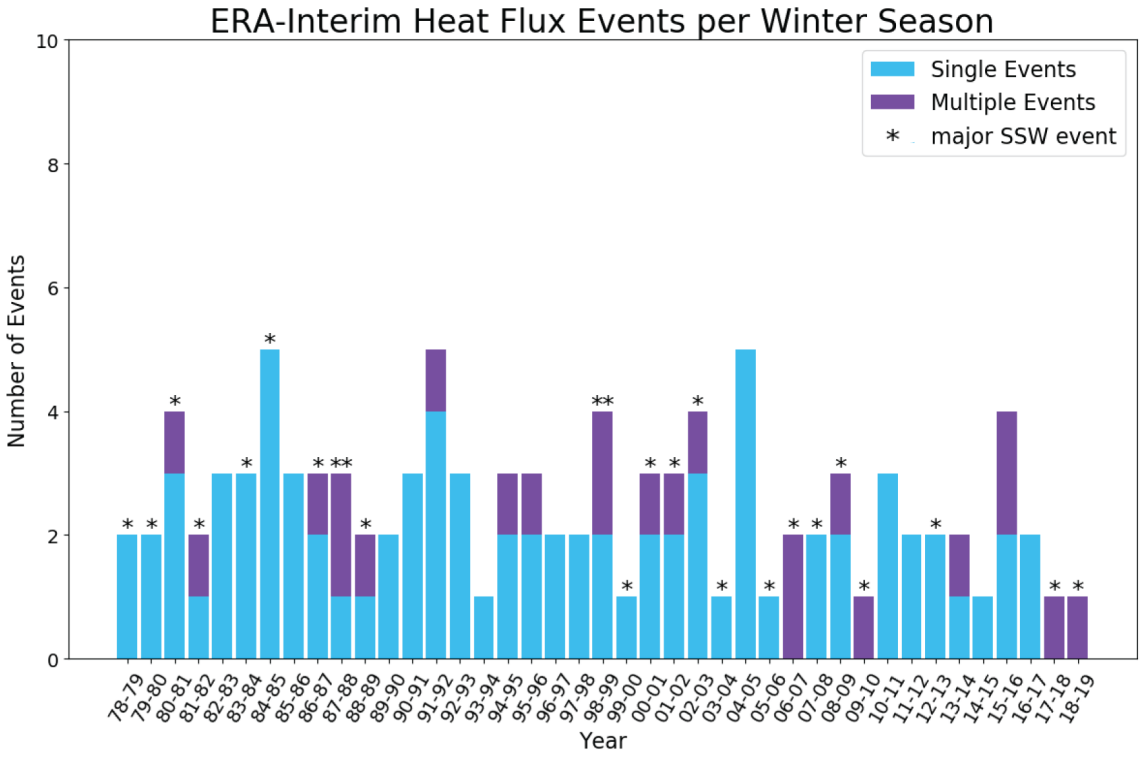

Figure 2.2: Reanalysis number of heat flux events per winter season for 81 single pulse events (blue) and 23 multiple pulse events (purple). Black stars indicated year or winter season in which a major SSW event occurred.

to visualize the interaction between the troposphere and stratosphere before, during and after the events. Similar plots could not be produced with the hindcast models as their length is too short. In order to get the multi-model mean, a mean was taken across each ensemble member within each model to form an ensemble mean, then a mean was taken across the models to form the multi-model mean. Patterns identified during and after the event can help describe the spatial characteristics of each wave pulse event such as: how long they last, in which particular regions their impact is the greatest, and what type of impact they have on the stratospheric polar vortex. Patterns before the start of the event are explored for their utility in forecasting such events with different patterns. Composite significance is done using a two-sided Student t-test at the 95% confidence interval except for the multi-model mean plots

where significance is determined by 5 out of 6 models having the same sign anomaly at a particular grid point.

Chapter 3

Characteristics of Single and Multiple Wave Pulse Events

In this chapter, we investigate the differences in wave pulse events and the impact they have on the stratospheric polar vortex. The goal is to identify key characteristics that make these single and multiple wave pulse events different from each other, such as duration, intensity, and impact. We use a bottom-up approach starting with tropospheric patterns that can amplify these atmospheric waves and then discuss the impacts on the stratosphere and end with a vertical representation of the waves with time. This chapter focuses on reanalysis events and later (Chapter 4) we will examine S2S model events.

3.1 Single vs. Multiple Pulses in Reanalysis

3.1.1 Spatial Geopotential Height and Heat Flux Patterns

First, to understand the spatial features that are associated with the vertically propagating waves, we look at 500 hPa geopotential height (GPH) anomalies (Fig. 3.1) and 100 hPa meridional heat flux anomalies (Fig. 3.2) associated with reanalysis single and multiple pulse events. For single pulse events, the Day -5 GPH pattern is indicative of a dominant wave-1 pattern with an anomalous ridge building over Eurasia and the North Atlantic and negative height anomalies over the North Pacific and spreading over the Arctic region (Fig. 3.1a). The Eurasian ridge has been mentioned in multiple studies preceding polar vortex disruptions as the Ural high (e.g. Cohen and Jones, 2011; Karpechko et al., 2018; Peings, 2019). The anomalous trough over the North Pacific is also very important for enhancing the meridional heat flux as seen in the climatology of heat flux over the North Pacific (Fig. 1.2). However, the

wave-1 mid-tropospheric height pattern does not amplify the Day -5 lower stratospheric vertical wave activity as seen in Figure 3.2a, where equal areas of positive and negative meridional heat flux anomalies exist over the Northern Hemisphere. The original wave-1 GPH pattern (Fig. 3.1a) evolves into a wave-2 pattern over the Northern Hemisphere thereafter (Fig. 3.1b). The North Pacific trough evolves into a trough-ridge pattern on Day 0 (i.e., the start date) of the events (Fig. 3.1b), with a ridge located over Alaska and a trough over eastern Siberia. Moreover, the anomalous ridging over the North Atlantic into central Eurasia remains stationary through the start day of the single pulse events. On Day 0, these mid-tropospheric features amplify the background planetary wave field and are associated with three well-defined regions of significant positive heat flux (Fig. 3.2b). These three regions are the North Pacific, Central Eurasia, and the North Atlantic/Northwest Europe. The trough-ridge pattern over the North Pacific appears to be a driving mechanism for the heat flux anomalies that occur over this region (Fig. 3.2b). Moreover, the anomalous ridging over the North Atlantic into central Eurasia is also the focal point for the heat flux anomalies in those two regions as well.

Since the ridging over Eurasia and the North Atlantic remains relatively stationary for more than five days, it may be the indication of a blocking pattern across the Northern Hemisphere. Atmospheric blocks often increase vertical wave activity into the stratosphere as seen here on Day 0 of the single pulse events as they amplify the background stationary wave pattern (Fig. 3.2b; Attard and Lang, 2019; Peings, 2019). Moving through Day +5 and Day +10, the wave-2 pattern breaks down. The trough-ridge pattern in the North Pacific is replaced by an anomalous ridge and the Eurasian ridge replaced with anomalous troughing over Greenland and Northern Europe (Figs. 3.1c-d). Associated with this height pattern, there is little resemblance remaining in the previous amplified heat flux pattern outside of the North Pacific and Northern Europe which still has positive heat flux anomalies occurring (Fig. 3.2c).

The decrease in positive heat flux is expected as most single pulse events are relatively short lived. Heat flux anomalies are predominantly negative at 100 hPa ten days after the initial pulse (Fig. 3.2d).

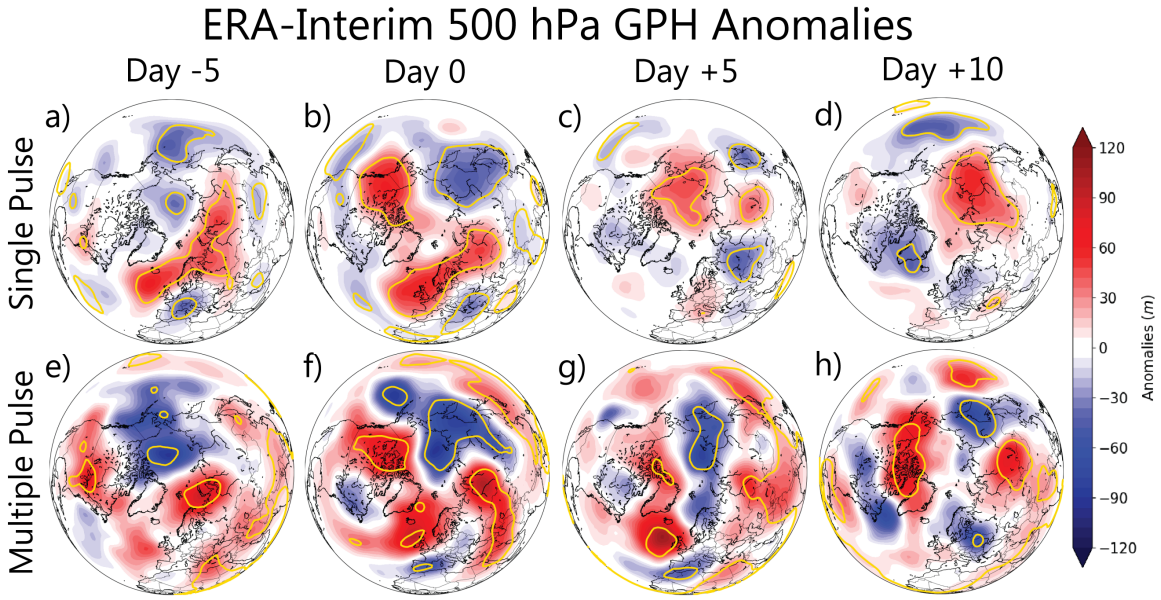

Figure 3.1: Lag composites of 500 hPa geopotential height anomalies (m) for (top) 81 single pulse events and (bottom) 23 multiple pulse events from Day -5 to Day +10 and Day 0 being the start day of the events. Statistical significance ($p < 0.05$) done using a two-sided Student t-test. Statistical significance indicated by the gold contour.

When looking at reanalysis multiple pulse events (Figs. 3.1e-h), we see a similar pattern to that of the single pulse events with an anomalous trough occurring in the North Pacific region and a much less spatially spread ridge developing over northern Eurasia prior to the event on Day -5 (Fig. 3.1e). The anomalous trough in the North Pacific remains relatively stationary through Day 0 (Fig. 3.1f). On the other hand, anomalous ridging expands in area from Northern Eurasia into North America. Nonetheless, there is a dominant wave-1 pattern over the Arctic region on Day 0 (Fig. 3.1f). As previously mentioned, a wave-1 pattern amplifies the vertical wave activity into the stratosphere as seen in Figure 3.2f. The ridging over central

Asia and the North Atlantic as well as the trough in the North Pacific enhance vertically propagating waves into the stratosphere as they are co-located with significant positive heat flux anomalies on Day 0 of multiple pulse events (Fig. 3.2f). The three regions with increased meridional heat flux are the same well defined regions seen in single pulse events (Fig. 3.2b). However, the Day -5 to Day 0 GPH pattern is more stationary for multiple pulse events than the pattern seen in the single pulse events which evolves into the wave-2 pattern. The Eurasian ridge associated with single pulse events lasts through Day 0 but the ridge associated with multiple pulse events is persistent through Day +10. The North Pacific/eastern Siberia trough is also much more persistent lasting through Day +10 for multiple pulse events (Fig. 3.1h).

On Day +5 (Fig. 3.1g), the GPH pattern over Europe changes, with a trough located over Northern Europe and a ridge still located over the North Atlantic. Conversely, the trough over eastern Siberia and ridges over North America and central Asia still remain on Day +5. These stationary ridges are indicative of atmospheric blocks that occur during multiple pulse events. The long duration blocking pattern seen in Figures 3.1e-g for multiple pulse events leads to the amplification of the three regions of positive heat flux anomalies on Day 0 through Day +5. Atmospheric blocking ridges as well as the persistent trough over the North Pacific/eastern Siberia explains why multiple pulses are felt more in the stratosphere, as this blocking patterns amplifies vertically propagating waves for roughly twice as long as single pulse events. By Day +10 (Fig. 3.1h), ridging is still occurring over far North America and central Asia and a trough still located over eastern Siberia. The Eurasian ridge along with the North American ridge, although changing slightly in size and location, remain relatively stationary from Day 0 through Day +10. These trough-ridge characteristics associated with multiple pulse events suggest a wave-2 pattern, on Day +10, which continues to amplify the vertical wave flux into the stratosphere (Fig. 3.2h).

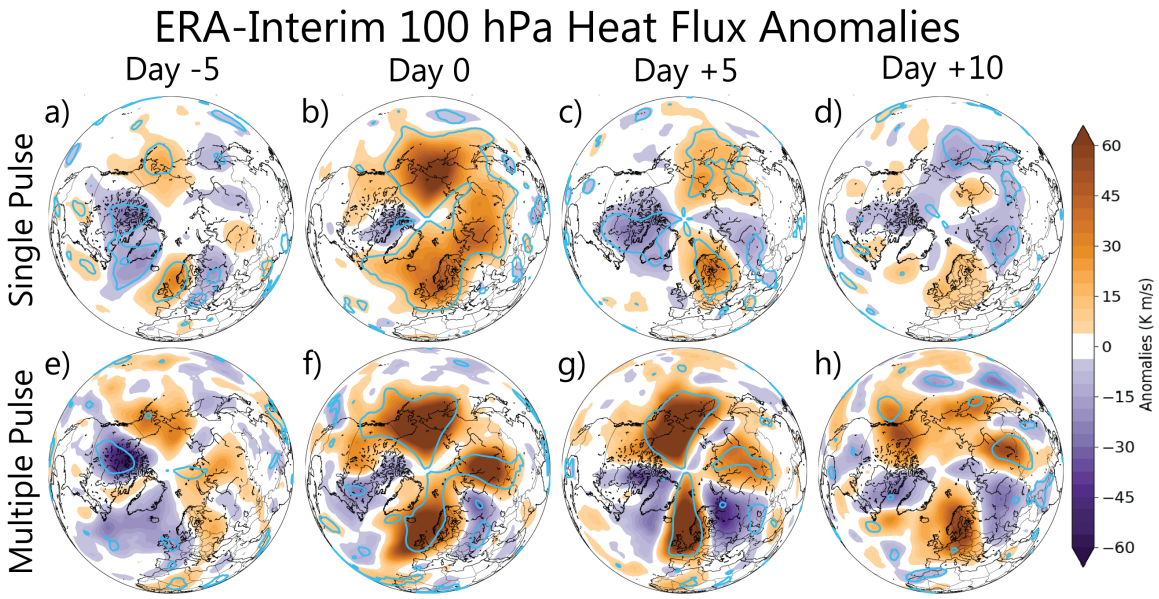

Figure 3.2: As in Fig. 3.1 but for 100 hPa heat flux anomalies (K ms^{-}1). Statistical significance ($p < 0.05$) done using a two-sided Student t-test indicated by the light blue contour.

3.1.2 Impact on the Stratospheric Polar Vortex

Next, we analyze the impact these vertically propagating waves have on the stratospheric polar vortex by examining the 10 hPa GPH (Fig. 3.3) as well as the 10 hPa zonal wind averaged for 60°N (Fig. 3.4). The 10 hPa level and 60°N latitude is often where the edge of the stratospheric polar vortex lies and therefore explains the disruptions in the polar vortex very well. Preceding both single (Fig. 3.3a) and multiple (Fig. 3.3e) pulse events, the polar vortex is anomalously strong based on negative height anomalies over the pole. The mean wind in the vortex preceding single pulse events is roughly 30 ms^{-1} (Fig. 3.4a). The vortex preceding multiple pulse events is much stronger at roughly 40 ms^{-1} (Fig. 3.4b). Along with a strong vortex, a ridge over Alaska also exists before Day 0. This anomalous height pattern represents a wave-1 pattern which weakens the polar vortex and pushes it over the Eurasian continent (e.g., Matsuno, 1970; Limpasuvan et al., 2004; Huang et al., 2018). The ridge over Alaska is much more expansive for multiple pulse events representing a

more amplified wave-1 pattern. A stronger vortex often makes it harder for waves to propagate into it, which may be why there is a more amplified wave-1 pattern before multiple pulse events as it takes a bigger wave to first disrupt the vortex. With time, the ridge pushes the vortex off the pole and over Eurasia where the vortex weakens (Figs. 3.3b and f). For both single and multiple pulse events, the winds within the polar vortex begin to weaken 2-3 days before the initial pulse (Day 0), with the greatest weakening occurring during the wave pulse event(s) (Figs. 3.4a and b). The development and intensification of the wave-1 GPH pattern is visible in both single and multiple pulse events (Figs. 3.3b and f). Where the single and multiple pulse events differ is after Day 0. Ten days after the initial pulse, the magnitude of positive height anomalies associated with single pulse events decreases, but increases for multiple pulse events (Figs. 3.3d and h). The decrease in magnitude of the significant anomalies for the single pulse events indicates less weakening of the vortex – i.e., a shorter lived disruption. Figure 3.4a shows a similar story with the vortex winds following single pulse events only weakening roughly 10 ms^{-1} and recovering within 10-15 days of the event.

In contrast, the expanding and deepening magnitude of these significant anomalies for multiple pulse events is evidence that the polar vortex continues to weaken 10 days after the initial event (Fig. 3.3h). Figure 3.4b supports this idea with the vortex winds continuing to decrease for 2-3 weeks after the initial pulse as the multiple wave pulse events continue to weaken the polar vortex. The vortex does not begin to recover until around 20 days after the initial wave pulse event. Figure 3.4b also hints that many multiple pulse events are major SSW events which is characterized by the 10 hPa wind dropping below zero (or becoming easterly) and confirmed in Figure 2.2. With multiple pulse events the 1-sigma spread drops below zero from Day 8 through Day 30 showing that numerous multiple pulse events are characterized as major SSWs. This is not the case for single pulse events as the 1-sigma spread gets

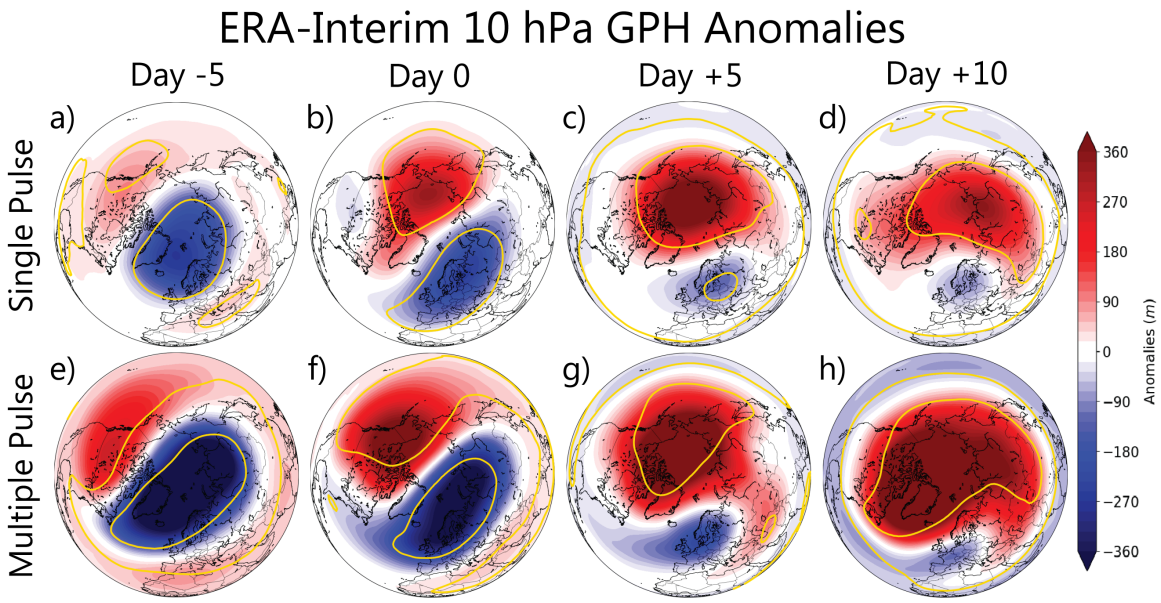

Figure 3.3: As in Fig. 3.1 but for 10 hPa geopotential height anomalies (m). Statistical significance ($p < 0.05$) done using a two-sided Student t-test indicated by the gold contour.

very close to, but never crosses, the zero line. Although the 1-sigma shading does not drop below the zero line, several single pulse events are characterized by a major SSWs. However, there is more consensus in multiple pulse events with a significant vortex weakening following the event than single pulse events. Therefore, most of the significant differences between the two events occur beyond the Day +10 window.

Further evidence of these differences can be seen in Figure 3.4c, which shows the mean wind difference of the polar vortex. To test how different the mean 10 hPa 60°N zonal wind is between the two events the difference between the means was taken and, using a two-sided Student t-test, statistical significance at the 95% confidence level was found on the difference indicated by the red line (Fig. 3.4c). Multiple pulse events are significantly stronger than single pulse events from Day -10 through Day +2. The two means are not significantly different during the rapid decrease in the wind speed just after Day 0. However, they become significantly difference once again as the multiple pulse events continue to impact the stratospheric polar vortex and decrease the wind speed, while the polar vortex following single pulse events starts to recover

around Day +10. The continued weakening following multiple pulse events lends more indication that multiple pulse events cause a statistically significant difference in the impact on the polar vortex from single pulse events. Thus, multiple pulse events have a greater, longer lasting impact on the stratospheric polar vortex than single pulse events, especially indicated by the growing area of significant positive height anomalies on Day +10 (Figs. 3.3d and h) and the mean wind difference after Day +10 (Fig. 3.4c).

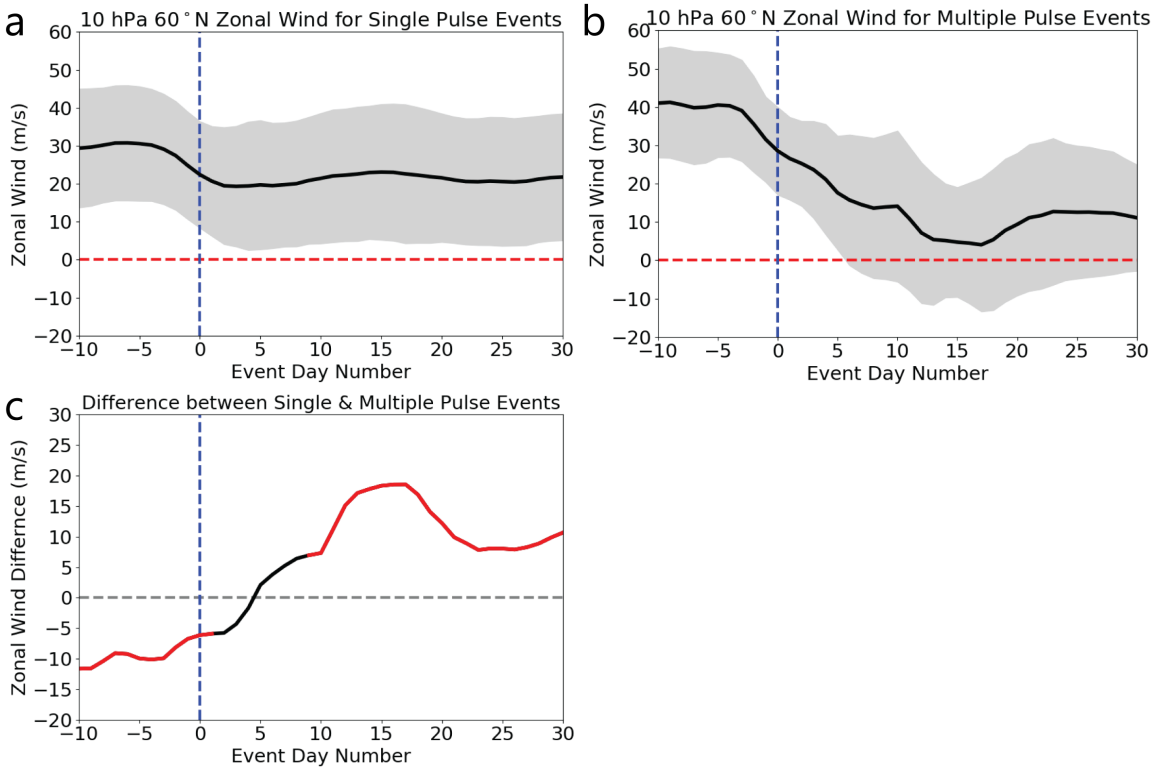

Figure 3.4: Time series of 10 hPa zonal wind from 60°N for (a) single pulse events, (b) multiple pulse events, and the (c) difference between them. (a,b) Grey shading indicates +/- one standard deviation around the event mean indicated by the solid black line. Vertical blue line indicated the identified start date of events and horizontal red line indicates the line of the wind being zero. Events that fall below the red line indicate a major SSW event occurred. Positive U-Wind values indicate a westerly wind and negative values indicate an easterly wind. (c) The difference between the mean line in a and b. The line is red when the difference in the two means is statistically significant using a two-sided Student t-test at the 95% confidence level.

3.1.3 Vertical Characteristics and Evolution

To tie the vertical propagation of waves and the disruption of the polar vortex together, we look at the vertical cross-sections of both the area-averaged meridional heat flux [v^*T^*] (40°N- 80°N) and GPH (60°N- 90°N) over time. Figures 3.5a and 3.5c show the vertical structure of the standardized heat flux associated with these events, represented as a composite of vertically propagating waves. Single pulse events last an average of 7 days, which is much shorter than multiple pulse events (12 days), consistent with our criteria. The greatest positive anomalies of the multiple pulse events occur in the middle and upper stratosphere, whereas the greatest positive anomalies for single pulse events occurs in the lower to middle stratosphere (Figure 3.5a and 3.5c). Stronger wave pulses further into the stratosphere results in a greater weakening of the polar vortex during and after multiple pulses events as there is more heat being fluxed into the polar vortex. Evidence of a weaker vortex following multiple pulse events can not only be seen in the wind difference (Fig. 3.4) but also in Figures 3.5b and 3.5d, which show the lag composite of GPH averaged over the polar cap (i.e., 60-90°N).

The standardized GPH anomalies associated with single pulse events initially have some upward expanse from the troposphere into the stratosphere during the wave driving event (i.e., Day 0 to +10) but lack substantial downward propagation at later lags (i.e., Days +20 and beyond) as they are relatively weak in magnitude. By contrast, the GPH anomalies associated with multiple pulse events are much greater in magnitude in the stratosphere and generally propagate downward with time, as seen by significant positive standardized GPH anomalies in the troposphere 15 to 45 days after the initial pulse occurs, similar to anomalies shown in Baldwin and Dunkerton (2001). The greater anomalies associated with multiple pulse events signal a weaker vortex as seen in Fig. 3.4b. Significant tropospheric GPH anomalies point towards the possibility of tropospheric weather pattern changes following multiple wave pulse

events. There are also statistically significant ($p < 0.05$) negative GPH anomalies in the stratosphere prior to single and multiple pulse events (Figs. 3.5b and d), indicating there is a relatively strong vortex before these events occur. As discussed later, a strong vortex may be important before polar vortex disruptions.

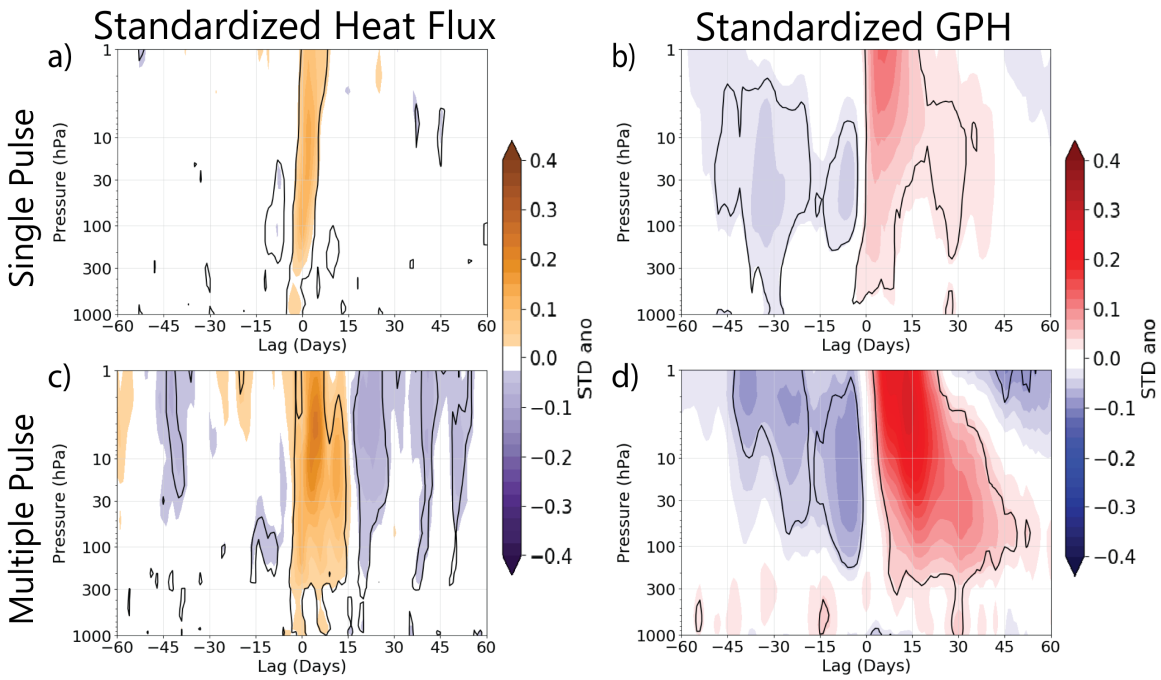

Figure 3.5: Lag composite of area-averaged (left) standardized heat flux (40°N- 80°N) and (right) standardized GPH (60°N- 90°N) from -60 to +60 days as a function of pressure (hPa). (a,b) Composites of 81 singe pulse events. (c,d) Composites of 23 multiple pulse events. Day 0 represents the start date of the event (see text). Statistical significance done using a two-sided Student t-test at the 95% confidence interval indicated by the black contour.

3.1.4 Discussion of Reanalysis Results

For the single pulse events, several features enhance the heat flux anomalies leading to the pulse events. The Alaskan ridge/Siberian trough axis, along with a Eurasian ridge (Fig. 3.1b), drive the heat flux on Day 0 (Fig. 3.2b). The development of the blocking high over the Urals may increase the potential for vertical wave activity for the events. For the multiple pulse events, the features that drive the heat flux

anomalies for the pulses (Figs. 3.2e-h) are a stationary eastern Siberian trough and Eurasian ridge from Days -5 through Days +10 (Figs. 3.1e-h) along with a North Atlantic ridge from Day 0 to Day +5 (Figs. 3.1f-g). The persistent blocking pattern seen in the multiple pulse events has been noted in several studies during anomalous vertical wave activity. Attard and Lang (2019) noted that blocking highs can enhance wave-1 patterns and extreme heat flux anomalies especially over the North Pacific as seen in this analysis. The same study also mentioned that blocks that occur outside of the North Pacific were associated with vortex displacements over Eurasia, agreeing with the findings in Figs. 3.3c-d and f-g. The 10 hPa heights also display, along with an initial wave-1 pattern, an anomalously strong polar vortex preceding the polar vortex disruption (Figs. 3.3a and e and 3.5b and d). Similar findings are mentioned in several studies preceding a polar vortex disruption (e.g. Karpechko et al., 2018; Lee et al., 2019b). An anomalously strong vortex preceding a disruption can limit the amount of waves that can propagate vertically into the stratosphere to large planetary waves such as wave-1 and wave-2 (e.g. Scott et al., 2004; Lawrence and Manney, 2020). Scott et al. (2004) also mentioned that a strong vortex may help to increase vertical wave propagation and wave breaking in the upper stratosphere which we show in Figures 3.5a and c with the largest standardized anomalies in the middle and upper stratosphere. The strong stratospheric polar vortex before single pulse events (Fig. 3.5b) appears to have some coupling with the troposphere as well possibly increasing the strength of the tropospheric jet and therefore influencing surface weather patterns.

Interestingly, there is a significant difference in the strength of the 10 hPa zonal winds (Fig. 3.4c) following single and multiple pulse events. The vortex is less weakened and thus recovers quicker following single pulse events (Fig. 3.4a). The multiple pulses and their impact on the vortex can be visualized relatively well with the several weakening periods of the polar vortex (Fig. 3.4b). The longevity of

multiple pulse events not only weakens the polar vortex more but also keeps the vortex weaker for about twice as long as single pulse events. The 10 hPa standardized GPH anomalies in Figures 3.5b and d slightly disagree with this statement as both show positive values from Day 0 to Day +40. Although, the higher magnitude positive anomalies lasts up to 20 days for single pulse events contrasted with up to 40 days for the multiple pulse anomalies. Creating a more substantial impact on the polar vortex may be the reason why stratospheric anomalies following multiple pulse events are greater than in single pulse events. The greater the anomalies and the longer they last gives them a better opportunity to downward propagate.

As shown by the standardized heat flux and the standardized GPH (Fig. 3.5), multiple pulse events are both longer lived and more intense wave driving events in the stratosphere than single pulse events. However, in order to more accurately compare the single and multiple pulse events, random samples of 23 events (i.e. equal to the number of multiple pulse events) were chosen from the single pulse events. We compare these random composites with the multiple pulse events (not shown). After inspection, no random selection of single pulse events looks distinctly similar to that of the multiple pulse events with the intensity and duration of the wave driving event or with the impact on the stratosphere GPH. Even the most extreme single pulse events did not replicate the impacts of multiple pulse events.

To reinforce the idea that multiple pulse events are fluxing more heat into the stratosphere, we summed the 100 hPa heat flux for each day within each of the reanalysis events (like those seen in Figure 2.1) and calculated the cumulative area-averaged heat flux for each event (Fig. 3.6). The start and end dates for each event of this summation are used from the first set of our criteria (i.e., the first and last day the meridional heat flux value surpassed the 500 and 100 hPa percentiles). We found multiple pulse events averaged nearly 100 $Kms^{-1}event^{-1}$ more that single pulse events. This cumulative heat flux difference demonstrates that the multiple

pulse events are fluxing much more heat into the stratospheric polar vortex, causing a greater disruption. Figure 3.6 also shows single or multiple pulse events that were associated with major SSW events as well (labeled with a triangle). Major SSWs are particularly intense events in that the mean of the cumulative meridional heat flux for major SSW events is higher than the other single or multiple pulse events. Thus, it makes sense that a slight majority of major SSW events occur with multiple pulse events, as seen in 10 hPa wind composites (Figs. 3.4a-b), as they are usually the event that produces this larger quantity of heat being fluxed into the stratosphere which leads to a greater disruption.

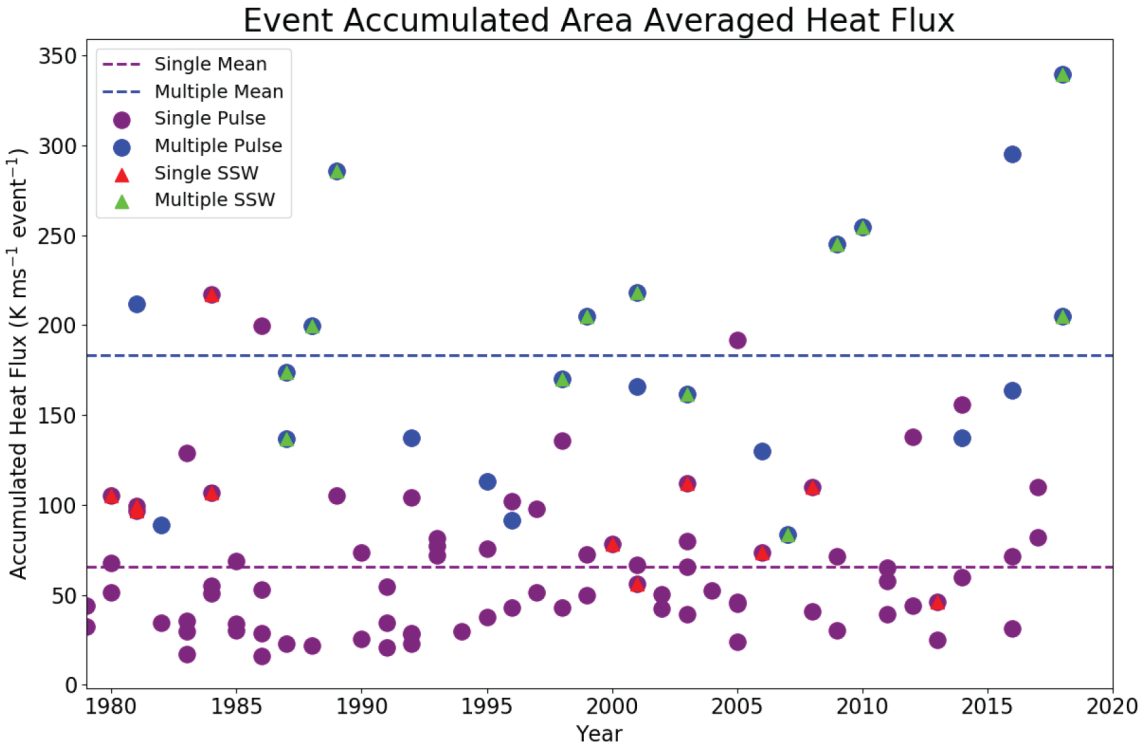

Figure 3.6: Cumulative area-averaged heat flux (K ms^{-1}) for each reanalysis event. Purple dots indicate single pulse events and blue dots indicate multiple pulse events. Lines of those respective colors indicate events mean. Triangles indicate major SSW events that are associated with a particular single (red) or multiple (green) pulse event.

Often mentioned in studies involving a weak or disrupted polar vortex is the surface temperature response in the form of Arctic air outbreaks, especially over Siberia

(Kolstad et al., 2010; Cohen and Jones, 2011; Kidston et al., 2015; Karpechko et al., 2018; Kretschmer et al., 2018). Looking at similar lag plots of surface temperatures surrounding single (Fig. 3.7) and multiple (Fig. 3.8) pulse events there is little in the way of any consistent significant cold pattern that evolves in the composites for the events. Central Siberia has the most consistent pattern of cold temperature anomalies which occurs leading up and during the event days (Figs. 3.7a-b and 3.8a-b). Starting Day 0 through day +10 of single pulse events (Figs. 3.7b-d), the warming of the Arctic region is very evident and correlates strongly with the rise in polar cap heights seen in the middle troposphere (Figs. 3.1b-d). Similar patterns can be seen associated with multiple pulse events with the warming of far northern North America and the Arctic region from Day -5 through Day +20 (Figs. 3.8a-f). The longer duration of positive temperature anomalies over the Arctic region corresponds to the prolonged weakening of the weaker vortex that is associated with multiple pulse events. However, 10-30 days following both the single and multiple pulse events there is little in the way of a consistent cold pattern which is often seen following a weakened vortex, especially over Eurasia. The lack of cold anomalies is surprising, especially following multiple pulse events, as the mean vortex is very weak for up to 20 days (Fig. 3.4b). Multiple pulse events are also associated with downward propagating stratospheric GPH anomalies into the troposphere (Fig. 3.5d) which have been shown to cause cold air outbreaks over Eurasia in other studies (e.g., Cohen et al., 2007; Kretschmer et al., 2018).

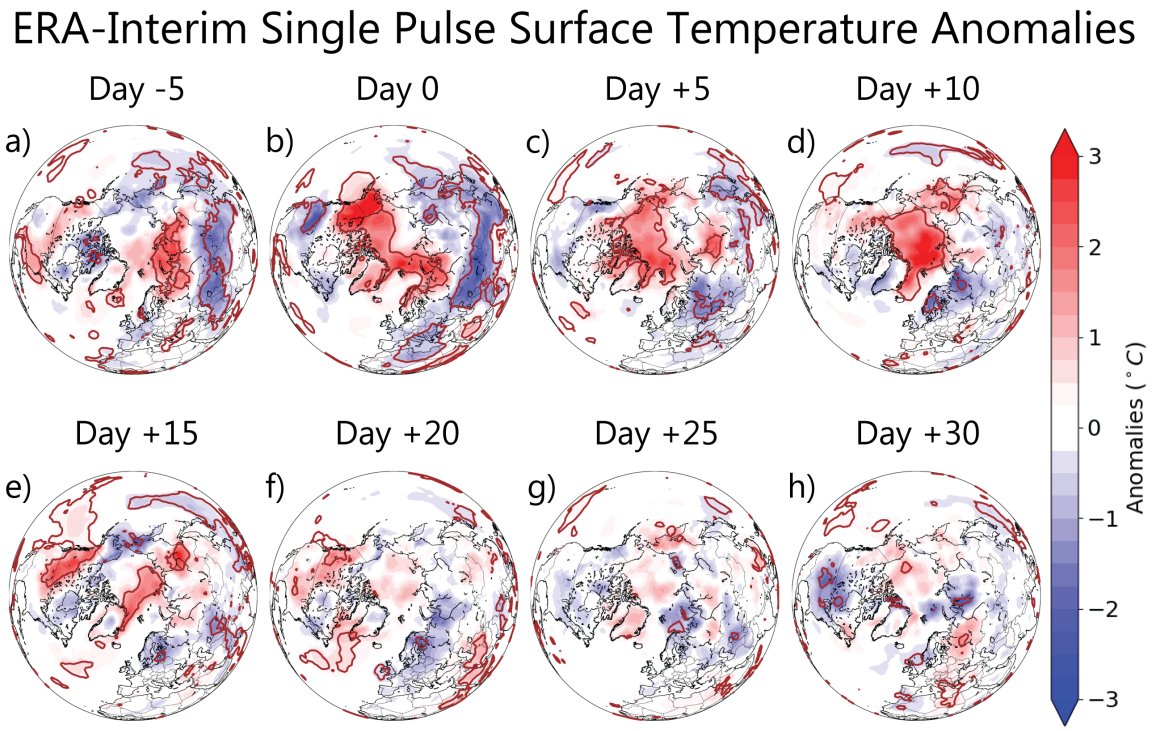

Figure 3.7: Lag composite of surface temperature anomalies (°C) for 81 single pulse events from Day -5 to Day +30 and Day 0 being the start day of the events. Statistical significance ($p < 0.05$) done using a two-sided Student t-test. Statistical significance indicated by the brown contour.

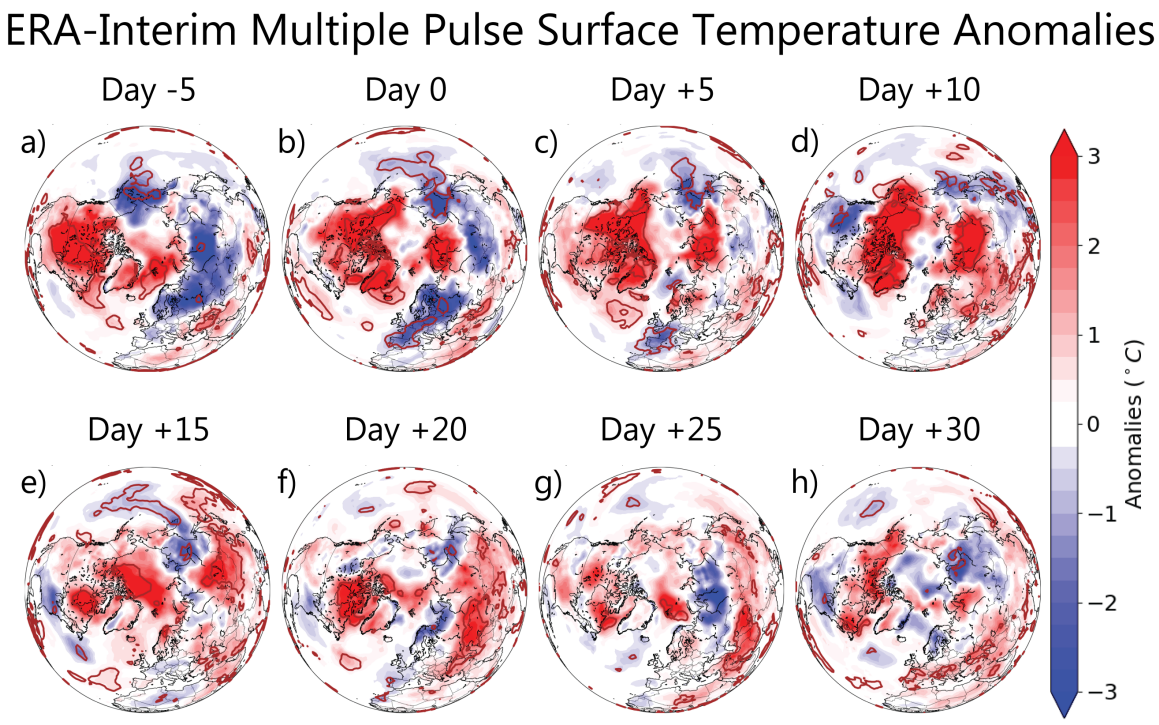

Figure 3.8: As in Fig. 3.7 but for 23 multiple pulse events.

Chapter 4

Single vs. Multiple Pulses in S2S Models and Origin of Wave Pulses

Thus far, we have examined atmospheric characteristics, both spatially and vertically, that occur before, during, and after single and multiple wave pulse events in reanalysis. However, we have yet to discuss how S2S operational models produce such events and identify the locations for which these wave pulses most often occur. Using the models not only increases the sample size of our wave pulse events but also increases the possible outcomes for patterns that produce wave pulses, helping to identify the important patterns driving these events. In this chapter, we compare and contrast the spatial patterns seen in Chapter 3 with that of S2S models in a multi-model mean. We also analyze four separate regions across the Northern Hemisphere in which wave pulse events are likely to occur, including how often the multiple pulses occur in the same region. Knowing the location of wave pulse events and the tropospheric weather patterns that accompany them, such as stationary troughs and blocking highs, could help in the S2S forecasting of wave pulse events and subsequently the impact on the stratospheric polar vortex and its downward influences.

4.1 Single vs. Multiple Pulses in S2S Hindcast Models

4.1.1 Tropospheric Spatial Geopotential Height Patterns

We first investigate 500 hPa GPH anomalies before and after wave pulse events in several S2S hindcasts (Fig. 4.1). Note that the colorbar seen in Fig. 4.1 is half of that used for the reanalysis events. This change was done to resolve the pattern better as there are many more samples associated with the S2S models and thus more

smoothing occurs during the compositing process. For our multi-model mean of single pulse events (Fig. 4.1a), the Day -5 pattern is similar to that of reanalysis events with dominant wave-1 pattern with an anomalous ridge building over Eurasia and the North Atlantic and negative height anomalies over the North Pacific. This North Pacific trough evolves into a trough-ridge pattern on Day 0 of the events (Fig. 4.1b), as seen in reanalysis single pulse events (Figs. 3.1a-b). As previously mentioned, the Eurasian ridge and Pacific trough helps to amplify vertical wave activity over the North Pacific region for wave pulse events as seen in Fig. 4.2b. The wave-1 pattern evolves similarly to reanalysis into a wave-2 pattern over the Northern Hemisphere on Day 0 through Day +5 (Figs. 4.1b-c). However, the wave-2 pattern in the multi-model mean is different from the pattern on Day +5 in reanalysis (Fig. 3.1c) as reanalysis has an anomalous ridge over the North Pacific and into the Arctic region. By Day +10 (Fig. 4.1d), the multi-model mean again looks similar to reanalysis (Fig. 3.1d) with an anomalous ridge over the North Pacific into the Arctic region and anomalous troughing in North America and Northern Europe.

Furthermore, when looking at multi-model mean of multiple pulse events GPH pattern (Figs.4.1e-h), we see a similar pattern to that of reanalysis multiple pulse events – an anomalous trough occurring in the North Pacific region and a ridge developing over northern Eurasia prior to the event on Day -5 (Fig. 4.1e). The anomalous trough deepens and grows in spatial extent over the North Pacific and into eastern Siberia on Day 0 (Fig. 4.1f). The multi-model mean slightly varies from reanalysis on Day 0 with the troughing feature being much more expansive, reaching into North America. The anomalous ridging also expands in area from Northern Eurasia into North America. The stationarity and deepening of this pattern suggests the atmosphere is being blocked due to the Eurasian ridge. The atmospheric block leads to a wave-1 pattern over the Arctic region on Day 0 (Fig. 4.1f). The wave-1 pattern is more stationary and expansive than the pattern seen in the single pulse

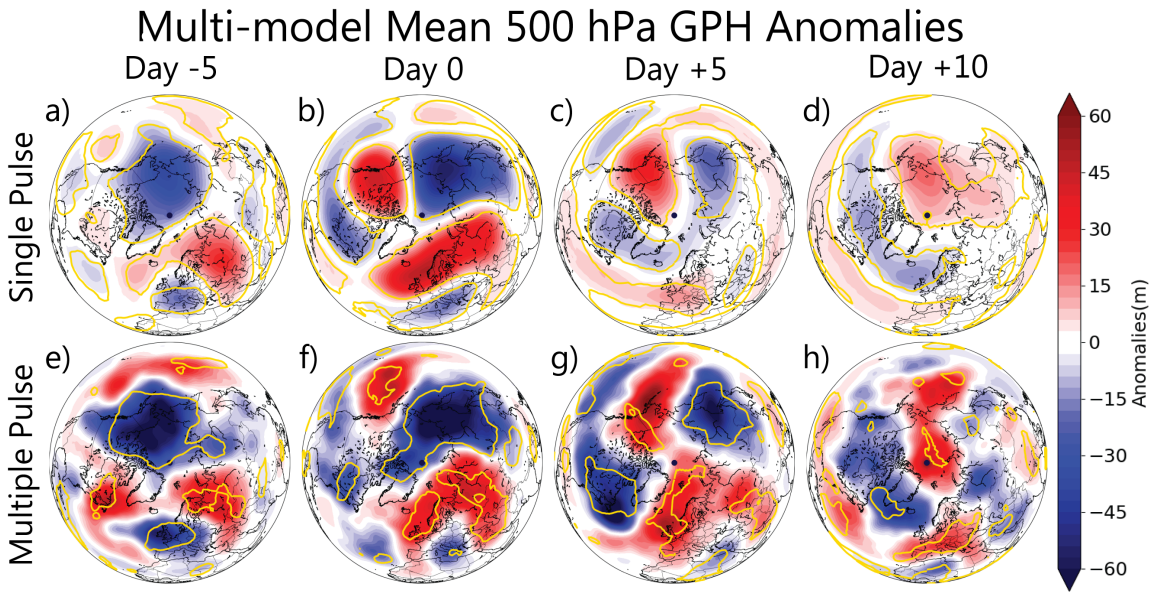

Figure 4.1: As in Fig. 3.1 but multi-model mean. Statistical significance for the multi-model mean found by 5 out of 6 models having same sign anomaly. Statistical significance indicated by the gold contour. Note that values on the colorbar are half of that displayed in Fig. 3.1.

events. On Day +5 (Fig. 4.1g), the pattern begins to develop into a wave-2 pattern which is different from that seen in the reanalysis multiple pulse events (Fig. 3.1g), with a trough-ridge pattern over the North Pacific region and another trough-ridge pattern over the North Atlantic. Although this pattern varies from reanalysis, it is still conducive to enhance vertically propagating waves as seen in the heat flux composite (Fig. 4.2g). On Day +10 the multi-model mean multiple pulse events looks very different from reanalysis multiple pulse events (Fig. 3.1h) as it does not capture the ridge or North America or over central Asia as well the the trough over eastern Siberia. The multi-model mean multiple pulse event pattern resembles more of a single pulse event pattern (Fig. 4.1d) with an anomalous ridge over the North Pacific and trough over the North Atlantic.

4.1.2 Stratospheric Spatial Heat Flux Pattern

Next, we look at the lower stratospheric spatial heat flux anomalies produced by the multi-model mean. Figure 4.2 displays the spatial maps of 100 hPa heat flux anomalies for the multi-model mean single and multiple pulse events. The multi-model mean single pulse events (Figs. 4.2a-d) are very similar to that of reanalysis (Figs. 3.2a-d) from Day -5 through Day +10. However, on Day 0 and on Day +5, the spatial extent of the heat flux anomalies for the multi-model mean encapsulates a slightly larger area which may be a result of more variability with more events. The decrease in positive heat flux by Day +5 through Day +10 (Figs. 4.2c-d) was also seen in the reanalysis single pulse events (Figs. 3.2c-d) suggesting similar short lived pulse events. The heat flux maps for the multi-model mean multiple pulse events (Figs. 4.2e-h) are similar to the spatial pattern of the reanalysis multiple pulse events (Figs. 3.2e-h). However, the multi-model mean disagrees with the reanalysis composite with little continuation of positive heat flux anomalies through Day +10 (Fig. 4.2h), which may indicate that model produced events may not be lasting as long as the events found in reanalysis. The differences in the Day +10 GPH pattern, with the lack of blocking highs, leads to differences in the duration of positive heat flux anomalies associated with multiple pulse events between reanalysis and the multi-model mean. The lack of positive heat flux anomalies on day +10 may also be due to the low sample size in most of the S2S models.

4.1.3 Impact on the Stratospheric Polar Vortex

Investigating the spatial height pattern at 10 hPa for the multi-model mean displays (Fig. 4.3) a very similar pattern to that of reanalysis (Fig. 3.3) for both single and multiple pulse events. A wave-1 pattern begins to emerge five days preceding the events with negative height anomalies over the pole, indicated by a strong polar vortex preceding the events, and a building ridge over Alaska and the North Pacific

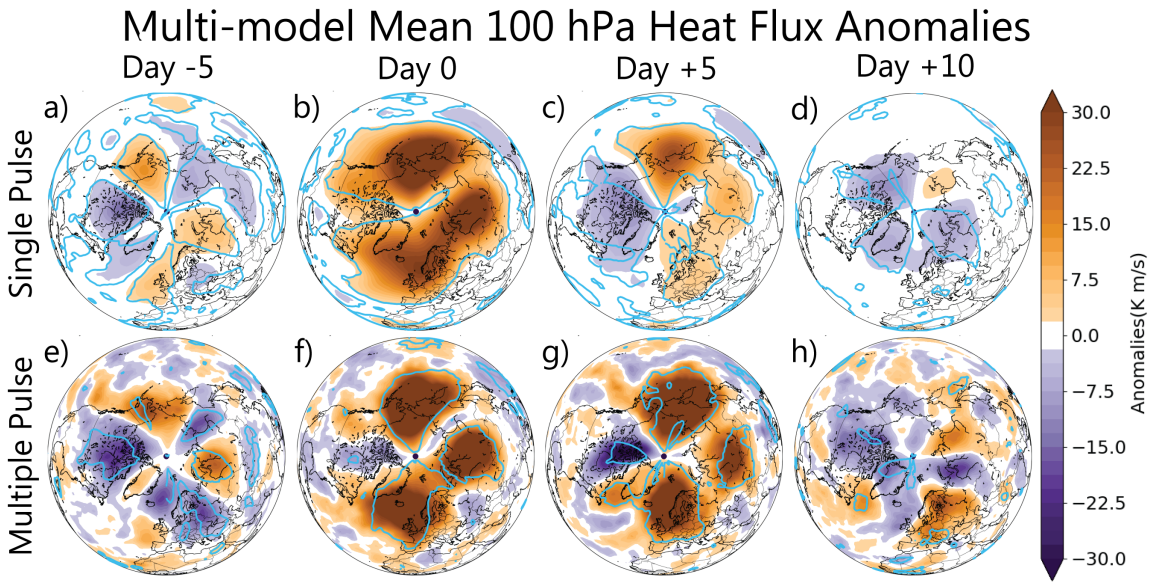

Figure 4.2: As in Fig. 3.2 but for the multi-model mean. Statistical significance for the multi-model mean found by 5 out of 6 models having same sign anomaly. Statistical significance indicated by the light blue contour. Note that values on the colorbar are half of that displayed in Fig. 3.2.

(Fig. 4.3a and e). The wave-1 pattern for the multiple pulse events is again slightly more amplified. The wave-1 pattern evolves similarly to reanalysis with the negative height anomalies decreasing in magnitude and moving over Northern Eurasia (Fig. 4.3b and f). Positive height anomalies dominate the polar region from 5-10 days following the events, indicating that the polar vortex is weakening and being shoved off the polar cap (Fig. 4.3c-d and g-h). The spatial extent and intensity of these anomalies is very comparable between both single and multiple pulse events produced by the multi-model mean with that of reanalysis. Once again the multiple pulse positive height anomalies grow in magnitude through Day +10 while the single pulse positive height anomalies weaken, indicating that multiple pulse events continue to weaken the polar vortex while the vortex starts to recover from the single pulse events.

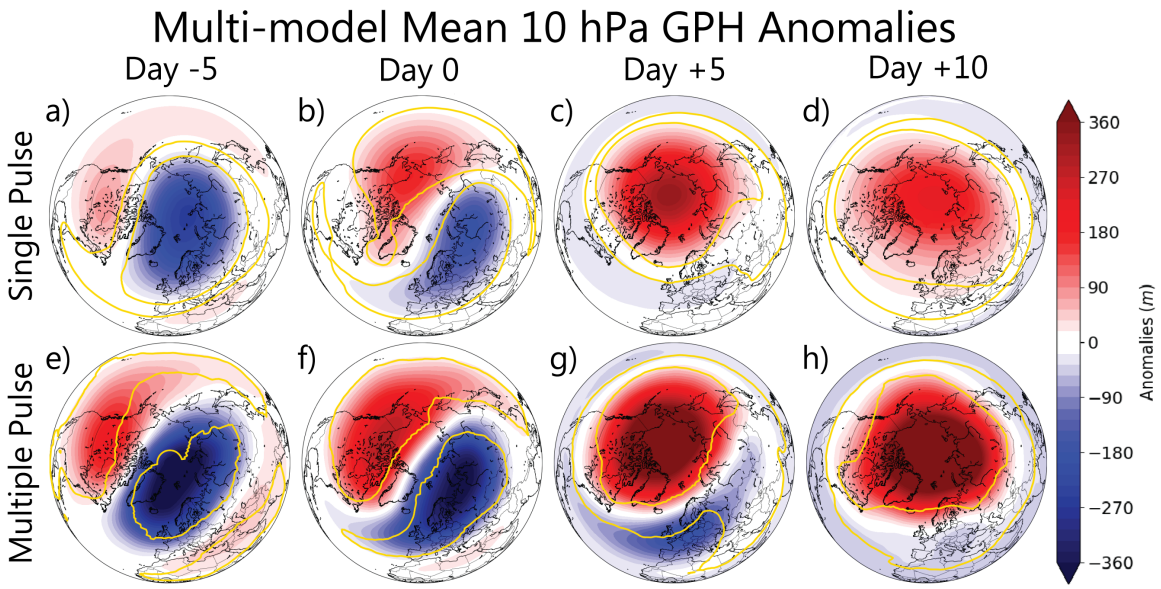

Figure 4.3: As in Fig. 3.3 but for multi-model mean. Statistical significance for the multi-model mean found by 5 out of 6 models having same sign anomaly. Statistical significance indicated by the gold contour.

4.2 Origin of Wave Pulse Events

Now, we take our investigation one step further and analyze the location of these wave pulse events. Knowing the location of the wave pulse events can help guide S2S forecasts to identify given patterns over certain regions which amplify vertically propagating waves that can impact the stratospheric polar vortex which is a source of increased skill for S2S forecasts (Butler et al., 2019; Domeisen et al., 2020b). To identify regions of origin for the pulses, we look at Figures 3.2 and 4.2 for guidance. There are 3 well-defined regions of anomalously positive heat flux/vertical wave propagation on Day 0 (Figs. 3.2 and 4.2, panels b and f). Thus, we divide the Northern Hemisphere from 40°N – 80°N into 4 equal-sized regions: (1) the European region (30°W - 60°E), (2) the Siberian region (60°E - 150°E), (3) the North Pacific region (150°E - 120°W), and (4) the North American region (120°W - 30°W) (Fig. 4.4). Within each region, we area-average the 100 hPa heat flux on Day 0. The region with the highest area-averaged heat flux value is labeled as the region where the wave

pulse originates. Regional maxima are also labeled to visualize spatially where pulses originated with just a red dot for single pulse events (Fig. 4.4a), and a red and blue dot for multiple pulse events (Fig. 4.4b). Area-averaging each region filters out small variability and allows for the identification of the strongest pulse(s) originating from larger waves that most impact the lower stratosphere.

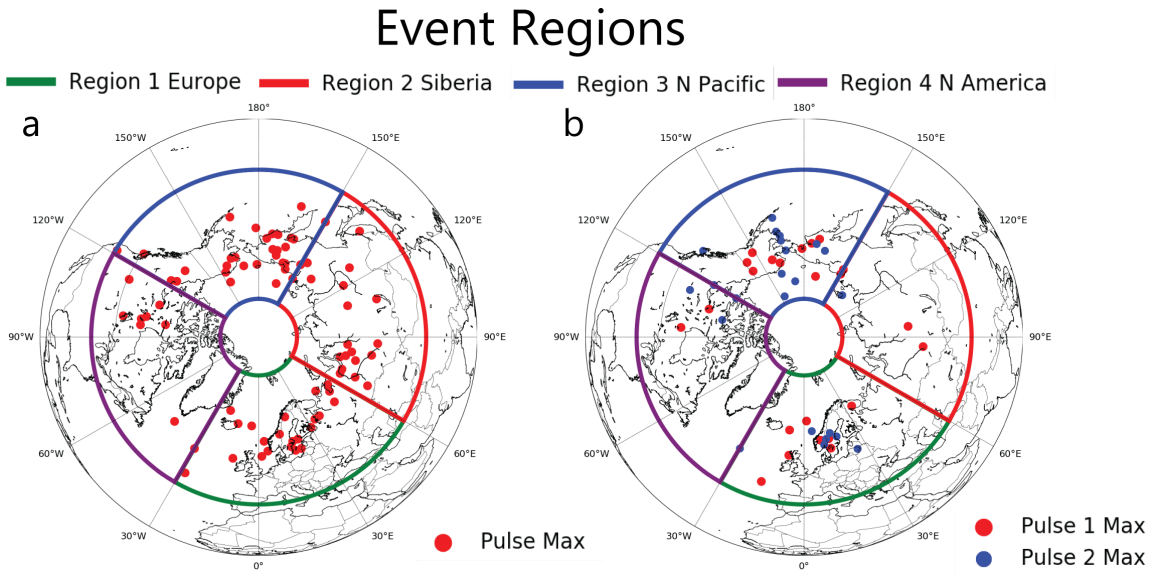

Figure 4.4: Origin of wave pulse events for single (left) and multiple (right) pulse events. Solid lines outline the individual regions of Europe (green), Siberia (red), North Pacific (blue), and North America (purple). Individual dots indicate the location of the maximum heat flux value inside the region found to contain the wave pulse event (maximum area-averaged heat flux). Red dots indicate the first pulse maximum (or only pulse for single pulse events) and blue dots indicate the second pulse maximum.

Tables 4.1-4.3 below display the occurrences of pulses in each region for each of the datasets. For single pulse events (Table 4.1), the North Pacific is on average the most favorable region for pulses to occur, with pulses occurring in this region roughly 30-38% of the time. The European and Siberian regions have the greatest variances between all of the datasets. Reanalysis, ECMWF, UKMO, and KMA have values of around 25% for both regions. However, NCEP slightly favors the European region at 34%, slightly higher than the North Pacific, and the Siberian region around

Table 4.1: Single pulse event region information for each dataset. N-value is total # of events found in each dataset. Percent based on number of events inside each region divided by the N-value in each dataset.

Region \ Dataset	ERA-Interim N=81	ECMWF N=1115	UKMO N=413	KMA N=374	NCEP N=1280	CMA N=4744	BOM N=14090
Europe	27.16%	27.62%	24.46%	24.33%	33.98%	16.82%	19.71%
Siberia	24.69%	23.68%	23.97%	22.73%	23.52%	34.17%	27.11%
North Pacific	37.04%	34.62%	35.84%	37.7%	31.17%	31.58%	36.54%
North America	11.11%	14.08%	15.74%	15.24%	11.33%	17.43%	16.64%

23.5%. In contrast, CMA and BOM have the European region less than 20% with the European region being the least favorable region in CAM. The Siberian region is the most favorable region in CMA at 34%, unlike other models. The region with the least frequency of pulses on average is the North American region, consistent with the signal in the spatial heat flux maps (Figs. 3.2 and 4.2).

For multiple pulse events (Table 4.2), the first pulse often originates in the North Pacific region, occurring roughly 30-40% of the time. The European region is a close second with pulses occurring around 30% of the time, except that the UKMO favors the European region much more than other models at 44%. Nonetheless, these two regions are very active synoptic wave regions and known for blocking events as well (Tibaldi and Molteni, 1990; Attard and Lang, 2019). As mentioned for single pulse events, CMA and BOM have much lower number in the European region than the other models by more than 10% at 19.5% and 18.6%, respectively. These same models favor the Siberian region by more than 10% from other models at 34.5% and 33%, respectively. Similarly, the North American region, on average, is the least common region for multiple pulses to occur. Reanalysis, however, shows that Siberia is the region with the fewest pulses for multiple pulse events. For the second pulse of the multiple pulse events (Table 4.3), there is a lot more variability in where these pulses occur. The increase in variability between models may be due to the low number of

Table 4.2: Same as Table 4.1 but for the first pulse of multiple pulse events.

Region \ Dataset	ERA-Interim N=23	ECMWF N=6	UKMO N=9	KMA N=12	NCEP N=11	CMA N=87	BOM N=333
Europe	34.78%	33.33%	44.44%	33.33%	27.27%	19.54%	18.62%
Siberia	8.7%	16.67%	22.22%	16.67%	18.18%	34.48%	33.03%
North Pacific	39.13%	33.33%	22.22%	33.33%	36.36%	31.03%	35.14%
North America	17.39%	16.67%	11.11%	16.67%	18.18%	14.94%	13.21%

events which can change the percentages greatly by adding an additional one or two events. However, the North Pacific in several datasets is the most common region and North America is the least common region.

We also investigate if the multiple pulse events are occurring in the same region (last row of Table 4.3), potentially signaling a stationary pattern that initiates multiple wave pulses within a common region that impact the stratosphere polar vortex over an extended period of time. We find in the reanalysis data, the first and second pulse of the multiple pulse events occur in the same region around 52% of the time while in the models around 33% of the time. The KMA and NCEP produce slightly higher percentages of 41.7% and 36.4%, respectively. The caveat to some of the model percentages is that they are based on a handful of events and adding one multiple pulse event could greatly increase or decrease this percentage. Yet, multiple pulses that occur in the same region may be an indication that between a third and half of the time, a stationary pattern may be responsible for driving multiple wave pulses which weaken of the polar vortex, which is consistent with large blocking highs or stationary troughs that often precede weak polar vortex events (Cohen and Jones, 2011; Karpechko et al., 2018; Kretschmer et al., 2018; Attard and Lang, 2019; Peings, 2019). The recurrence of pulses in the same region also points to the North Pacific and Eurasia often having a stationary feature, like the Pacific trough-Eurasian ridge pattern seen in Figs. 3.1b and 4.1b, leading multiple pulses to occur. Note that

Table 4.3: Same as Table 4.1 but for the second pulse of multiple pulse events. Last row indicates how often 1^{st} and 2^{nd} pulse occur in the same region.

Region \ Dataset	ERA-Interim N=23	ECMWF N=6	UKMO N=9	KMA N=12	NCEP N=11	CMA N=87	BOM N=333
Europe	26.09%	33.33%	22.22%	33.33%	45.45%	14.94%	14.11%
Siberia	4.35%	50%	44.44%	25%	18.18%	34.48%	33.03%
North Pacific	56.52%	16.67%	33.33%	25%	18.18%	33.33%	43.24%
North America	13.04%	0%	0%	16.67%	18.18%	17.24%	9.61%
$1^{st}/2^{nd}$ Pulse Same Region	52.17%	33.33%	33.33%	41.67%	36.36%	34.48%	33.93%

even though we are looking at multiple pulse events with only two pulses (the minimum) there are several multiple pulse events with 3 or more pulses that occur within the same event. Further analysis of these increased number of pulses is not done separately due to sample size.

4.2.1 Discussion of S2S Model Results and Pulse Origin

The S2S models analyzed here are very good at producing single pulse events and the spatial structures that occur with them are very similar to that of reanalysis. However, they lack proficiency at producing multiple pulse events as the number of those is significantly decreased compared to the number of single pulse events. Moreover, the spatial patterns that occur with the multiple pulse events are like that of the reanalysis with the dominant wave-1 or wave-2 pattern across the Arctic region. One possible reason for the lack of multiple pulse events in the models may be that the model runs themselves are not long enough to produce a robust multiple wave pulse as we cut off days at the beginning and end of each model run for compositing. Changing the criteria to be less strict at the 100 hPa level and for the peak criteria themselves was tried to increase the sample size. However, the models still lacked the capability to produce events. The criteria that created the greatest increase/decrease in events was altering the prominence criteria or how much a given point stands out

from its surrounding points, which may indicate that the amount of wave convergence in the lower stratosphere may be underpredicted in these S2S models. Models may also struggle in capturing the frequency and duration of atmospheric features, such as stationary troughs and blocking highs, which can be important in the amplification of vertical wave activity into the stratosphere for prolonged periods of time. Therefore, these parameters along with the struggle to produce atmospheric features may be the cause of few multiple pulse events as they are not able to fully capture some of the important features that drive multiple pulse events.

The inability of the S2S models to consistently produce multiple pulse events is currently a limitation. Since it was shown previously with the reanalysis data that multiple pulse events have a greater impact on the stratospheric polar vortex, our current operational S2S models may not be able to produce the full effect that such events may have on both the stratospheric polar vortex and the potential downward propagation of these events into the troposphere (e.g., Karpechko et al., 2018). Consequently, the possible surface impacts that accompany these events may also be predicted incorrectly. Therefore, this will result in reduced S2S forecast skill in association with stratosphere-troposphere coupling.

Several model biases appear to exist in the region the pulses occur. Tables 4.1-4.3 show the percentage of the total wave pulse events that originate with a given region. ERA-Interim, ECMWF, UKMO, KMA and NCEP datasets favor the European and North Pacific regions for wave pulse events to occur with the least favored region being North America. CMA and BOM datasets favor the Siberian and North Pacific regions for wave pulse events to occur instead. These differences can be seen in both single and multiple pulse events. Therefore, the models and reanalysis favor different regions for the production of wave pulse events. These biases may exist due to differences in the surface variability coupled within the model as well as the production of certain atmospheric features that help produce wave pulse events, as discussed previously.

Chapter 5

Summary and Conclusions

This thesis analyzed reanalysis data and several S2S hindcast model datasets to identify and characterize vertically propagating wave pulse events and how they impact the stratospheric polar vortex. Understanding the events that impact the stratospheric polar vortex is important as a weakened vortex can be a source for increased predictability on the S2S time frame (Robertson et al., 2015; Vitart et al., 2017; Vitart and Robertson, 2018; Lang et al., 2020). We create two sets of criteria to identify wave driving events from the troposphere into the stratosphere. The first set identifies days when there is wave driving. The second set looks at each of these wave driving events in more detail to identify the robust features in each wave driving event. These robust features are 'peaks' in the area-averaged meridional heat flux (40°N-80°N) which classify them as single and multiple wave pulse events depending on the number of peaks in each event.

We found that single wave pulse events are much shorter lived, as expected, and less intense events that multiple wave pulse events (Figs. 3.5a-d). The stratospheric polar vortex is more affected by multiple pulse events than single pulse events as seen in the 10 hPa 60°N zonal wind difference (Figs. 3.4c). Multiple pulse events also produce a similar looking downward propagating plot of stratospheric GPH anomalies (Fig. 3.5d) as that seen in Baldwin and Dunkerton (2001) and other studies. The downward propagation of stratospheric anomalies following multiple pulse events indicates that multiple pulse events are more likely to exhibit changes on the tropospheric jet and tropospheric weather patterns via downward propagation as well. Spatially, anomalous ridging (Figs. 3.1b-c and f-h) can be seen in both types of events which may enhance the heat flux occurring during the events (Figs. 3.2b-c and f-h) as well

as the wave-1 pattern that weakens and displaces the polar vortex (Figs. 3.3a-c). Furthermore, a stationary trough is seen in both events as well over the North Pacific that appears to be a key component in the enhanced heat flux during the events as well (Figs. 3.2e-h). The more persistent pattern associated with the multiple pulse events is what produces the prolonged enhancement of vertical wave activity and multiple wave pulses in the stratosphere.

S2S model hindcasts were used to check if patterns found in reanalysis were consistent when we increase the sample size and realistic outcomes for the production of single and multiple pulse events. Each ensemble member inside each model run during the winter months was investigated for wave pulse events. Models produce many more single pulse events than that of reanalysis. However, models struggle to produce multiple pulse events. We hypothesize the lack of multiple pulse events may be due to the length of the model runs being a limiting factor in producing these longer-lived events. Models also have the tendency to overpredict the strength of the stratospheric polar vortex which can lead to fewer waves propagating into the stratosphere limiting these multiple pulse events. The models also particularly struggled with producing stationary features associated with our events such as the anomalous trough over the North Pacific and the blocking highs over the Northern Hemisphere as well (Figs. 3.2e-h). Not being able to produce blocking highs or troughs will underestimate the amount of vertical wave activity being fluxed into the stratosphere and may limit the number of wave pulse events produced. Karpechko et al. (2018) describes something similar happening in the S2S models preceding the major SSW in 2018. The models were not able to predict the correct location of the Ural high which led to the underestimation of the vertical wave activity and eventually a poor prediction of the major SSW. Spatially, the multi-model mean was very similar to that of the reanalysis events on Day 0. Models are able to identify the three areas of robust heat flux on Day 0 (Figs. 4.1b and f) as well as both the and the 500 and 10

hPa GPH patterns and how they evolve surrounding the wave pulse events (Figs. 4.2 and 4.3). Although composites of the possible downward propagating effects as well as the zonal wind could not be produced because of the relatively short length of the hindcasts, it is encouraging that similar spatial patterns were produced.

Identifying the origin of the pulses was also important to this study as it can lend some increased S2S predictability when knowing common features that produce these wave pulse events and disrupt the polar vortex. Single pulse events appear to be driven by a trough-ridge dipole over the North Pacific which is favored for ∼33% of the wave pulse events (Figs. 3.1b and 4.1b). Single pulse events occur in both Europe and Siberia between 20-30% of the time in reanalysis, related to the anomalous ridging in these regions (Figs. 3.1b and 4.1b). Multiple pulse events also favor the North Pacific for pulses to occur due to the anomalous trough in this region (Figs. 3.1f and 4.1f). The second favored region for multiple pulse events is hard to identify across datasets due to the very small sample size. However, in the datasets that contain an appreciable number of events, Europe and Siberia are again the second and third favorite regions. Interestingly, both single and multiple pulse events favor the same regions for pulses to occur, leaving out the North American region with ∼10% of pulse events. These are the same regions highlighted in the climatology of heat flux as well (Fig. 1.2), due to the common storm tracks, planetary wave contribution, and mid-tropospheric patterns (i.e., blocking) that occur for each of the wave patterns and enhance the heat flux (Tibaldi and Molteni, 1990; Attard and Lang, 2019). More importantly, the multiple pulses occur in the same region >33% of the time in the models and ∼50% of the time in reanalysis which is a result of the stationary troughs and ridges associated with multiple pulse events.

Further investigation should be done into why models produce a very small amount of multiple pulse events as we have shown that these events cause the greatest impact

on the polar vortex and can be a source for increased S2S predictability. Stationary patterns such as atmospheric blocks seem to be the greatest issue for models to capture. Investigating more S2S models and comparing what parameters each model contains may help us understand the characteristics that lead a model to produce atmospheric blocks. It might also be useful to further examine reanalysis dates inside the models to see how each model represents those events as it may lend some increased understanding into what is lacking in the models. Models are particularly useful given the amount of outcomes they provide to a given scenario. Investigation of more individual wave pulse events and how certain models or certain ensemble members within the models produces an event could improve the knowledge of what creates or does not create a wave pulse event to occur. Being able to narrow down certain patterns within the models may eventually help increase the S2S predictability of these wave pulse events and their stratospheric impact.

Bibliography

Andrews, D. G., C. B. Leovy, and J. R. Holton, 1987: *Middle Atmosphere Dynamics*. Academic Press.

Attard, H. E. and A. L. Lang, 2019: Troposphere–stratosphere coupling following tropospheric blocking and extratropical cyclones. *Monthly Weather Review*, **147 (5)**, 1781–1804.

Baldwin, M. P. and T. J. Dunkerton, 1999: Propagation of the Arctic Oscillation from the stratosphere to the troposphere. *Journal of Geophysical Research: Atmospheres*, **104 (D24)**, 30 937–30 946.

Baldwin, M. P. and T. J. Dunkerton, 2001: Stratospheric harbingers of anomalous weather regimes. *Science*, **294 (5542)**, 581–584.

Barnston, A. G. and R. E. Livezey, 1987: Classification, seasonality and persistence of low-frequency atmospheric circulation patterns. *Monthly Weather Review*, **115 (6)**, 1083–1126.

Baxter, S. and S. Nigam, 2015: Key role of the North Pacific Oscillation–west pacific pattern in generating the extreme 2013/14 north american winter. *Journal of Climate*, **28 (20)**, 8109–8117.

Brunet, G., et al., 2010: Collaboration of the weather and climate communities to advance subseasonal-to-seasonal prediction. *Bulletin of the American Meteorological Society*, **91 (10)**, 1397–1406, doi:10.1175/2010BAMS3013.1.

Butler, A. H., A. Charlton-Perez, D. I. Domeisen, I. R. Simpson, and J. Sjoberg, 2019: Predictability of Northern Hemisphere final stratospheric warmings and their surface impacts. *Geophysical Research Letters*, **46 (17-18)**, 10 578–10 588.

Butler, A. H., J. P. Sjoberg, D. J. Seidel, and K. H. Rosenlof, 2017: A sudden stratospheric warming compendium.

Cai, M., Y. Yu, Y. Deng, H. M. van den Dool, R. Ren, S. Saha, X. Wu, and J. Huang, 2016: Feeling the pulse of the stratosphere: An emerging opportunity for predicting continental-scale cold-air outbreaks 1 month in advance. *Bulletin of the American meteorological Society*, **97 (8)**, 1475–1489.

Cassou, C., 2008: Intraseasonal interaction between the Madden–Julian Oscillation and the North Atlantic Oscillation. *Nature*, **455 (7212)**, 523–527.

Charney, J. and P. Drazin, 1961: Propagation of planetary scale waves from the lower atmosphere to the upper atmosphere. *J Geophys Res*, **66**, 83–109.

Chen, P. and W. A. Robinson, 1992: Propagation of planetary waves between the troposphere and stratosphere. *Journal of the Atmospheric Sciences*, **49 (24)**, 2533–2545.

Christiansen, B., 2001: Downward propagation of zonal mean zonal wind anomalies from the stratosphere to the troposphere: Model and reanalysis. *Journal of Geophysical Research: Atmospheres*, **106 (D21)**, 27 307–27 322.

Cohen, J., M. Barlow, P. J. Kushner, and K. Saito, 2007: Stratosphere–troposphere coupling and links with eurasian land surface variability. *Journal of Climate*, **20 (21)**, 5335–5343.

Cohen, J., J. C. Furtado, J. Jones, M. Barlow, D. Whittleston, and D. Entekhabi, 2014: Linking siberian snow cover to precursors of stratospheric variability. *Journal of Climate*, **27 (14)**, 5422–5432.

Cohen, J. and J. Jones, 2011: Tropospheric precursors and stratospheric warmings. *Journal of climate*, **24 (24)**, 6562–6572.

Dee, D. P., et al., 2011: The ERA-Interim reanalysis: Configuration and performance of the data assimilation system. *Quarterly Journal of the Royal Meteorological Society*, **137 (656)**, 553–597.

Domeisen, D. I., 2019: Estimating the frequency of sudden stratospheric warming events from surface observations of the North Atlantic Oscillation. *Journal of Geophysical Research: Atmospheres*, **124 (6)**, 3180–3194.

Domeisen, D. I., A. H. Butler, K. Fröhlich, M. Bittner, W. A. Müller, and J. Baehr, 2015: Seasonal predictability over europe arising from El Niño and stratospheric variability in the MPI-ESM seasonal prediction system. *Journal of Climate*, **28 (1)**, 256–271.

Domeisen, D. I., C. I. Garfinkel, and A. H. Butler, 2019: The teleconnection of El Niño Southern Oscillation to the stratosphere. *Reviews of Geophysics*, **57 (1)**, 5–47.

Domeisen, D. I., C. M. Grams, and L. Papritz, 2020a: The role of North Atlantic-European weather regimes in the surface impact of sudden stratospheric warming events. *Weather and Climate Dynamics Discussions*, 1–24.

Domeisen, D. I., et al., 2020b: The role of the stratosphere in subseasonal to seasonal prediction: 2. predictability arising from stratosphere-troposphere coupling. *Journal of Geophysical Research: Atmospheres*, **125 (2)**, e2019JD030 923.

Edmon Jr, H., B. Hoskins, and M. McIntyre, 1980: Eliassen-palm cross sections for the troposphere. *Journal of the Atmospheric Sciences*, **37 (12)**, 2600–2616.

Garfinkel, C. I., S. B. Feldstein, D. W. Waugh, C. Yoo, and S. Lee, 2012: Observed connection between stratospheric sudden warmings and the Madden-Julian Oscillation. *Geophysical Research Letters*, **39 (18)**.

Green, M. R. and J. C. Furtado, 2019: Evaluating the joint influence of the Madden-Julian Oscillation and the stratospheric polar vortex on weather patterns in the Northern Hemisphere. *Journal of Geophysical Research: Atmospheres*.

Haynes, P. H., M. McIntyre, T. Shepherd, C. Marks, and K. P. Shine, 1991: On the "downward control" of extratropical diabatic circulations by eddy-induced mean zonal forces. *Journal of the Atmospheric Sciences*, **48 (4)**, 651–678.

Huang, J., W. Tian, L. J. Gray, J. Zhang, Y. Li, J. Luo, and H. Tian, 2018: Preconditioning of arctic stratospheric polar vortex shift events. *Journal of Climate*, **31 (14)**, 5417–5436.

Jaiser, R., K. Dethloff, and D. Handorf, 2013: Stratospheric response to Arctic sea ice retreat and associated planetary wave propagation changes. *Tellus A: Dynamic Meteorology and Oceanography*, **65 (1)**, 19 375.

Jennrich, G. C., J. C. Furtado, J. B. Basara, and E. R. Martin, 2020: Synoptic characteristics of 14-day extreme precipitation events across the United States. *Journal of Climate*, **(2020)**.

Jucker, M. and T. Reichler, 2018: Increased predictability of sudden stratospheric warmings. *EGU General Assembly Conference Abstracts*, Vol. 20, 19442.

Karpechko, A. Y., A. Charlton-Perez, M. Balmaseda, N. Tyrrell, and F. Vitart, 2018: Predicting sudden stratospheric warming 2018 and its climate impacts with a multimodel ensemble. *Geophysical Research Letters*, **45 (24)**, 13–538.

Karpechko, A. Y., P. Hitchcock, D. H. Peters, and A. Schneidereit, 2017: Predictability of downward propagation of major sudden stratospheric warmings. *Quarterly Journal of the Royal Meteorological Society*, **143 (704)**, 1459–1470.

Kidston, J., A. A. Scaife, S. C. Hardiman, D. M. Mitchell, N. Butchart, M. P. Baldwin, and L. J. Gray, 2015: Stratospheric influence on tropospheric jet streams, storm tracks and surface weather. *Nature Geoscience*, **8 (6)**, 433–440.

Kim, B.-M., S.-W. Son, S.-K. Min, J.-H. Jeong, S.-J. Kim, X. Zhang, T. Shim, and J.-H. Yoon, 2014: Weakening of the stratospheric polar vortex by Arctic sea-ice loss. *Nature Communications*, **5 (1)**, 1–8.

Kim, H., J. H. Richter, and Z. Martin, 2019: Insignificant QBO-MJO prediction skill relationship in the SubX and S2S subseasonal reforecasts. *Journal of Geophysical Research: Atmospheres*, **124 (23)**, 12 655–12 666.

Kolstad, E. W., T. Breiteig, and A. A. Scaife, 2010: The association between stratospheric weak polar vortex events and cold air outbreaks in the Northern Hemisphere. *Quarterly Journal of the Royal Meteorological Society*, **136 (649)**, 886–893.

Kretschmer, M., D. Coumou, L. Agel, M. Barlow, E. Tziperman, and J. Cohen, 2018: More-persistent weak stratospheric polar vortex states linked to cold extremes. *Bulletin of the American Meteorological Society*, **99 (1)**, 49–60.

Lang, A. L., K. Pegion, and E. A. Barnes, 2020: Introduction to special collection:"bridging weather and climate: Subseasonal-to-seasonal (S2S) prediction". *Journal of Geophysical Research: Atmospheres*, **125 (4)**, e2019JD031 833.

Lawrence, Z. D. and G. L. Manney, 2020: Does the Arctic stratospheric polar vortex exhibit signs of preconditioning prior to sudden stratospheric warmings? *Journal of the Atmospheric Sciences*, **77 (2)**, 611–632.

Lee, S., J. Furtado, and A. Charlton-Perez, 2019a: Wintertime North American weather regimes and the Arctic stratospheric polar vortex. *Geophysical Research Letters*.

Lee, S. H., A. Charlton-Perez, J. Furtado, and S. Woolnough, 2019b: Abrupt stratospheric vortex weakening associated with North Atlantic anticyclonic wave breaking. *Journal of Geophysical Research: Atmospheres*, **124 (15)**, 8563–8575.

Lim, E.-P., H. H. Hendon, G. Boschat, D. Hudson, D. W. Thompson, A. J. Dowdy, and J. M. Arblaster, 2019: Australian hot and dry extremes induced by weakenings of the stratospheric polar vortex. *Nature Geoscience*, **12 (11)**, 896–901.

Lim, Y., S.-W. Son, and D. Kim, 2018: Mjo prediction skill of the subseasonal-to-seasonal prediction models. *Journal of Climate*, **31 (10)**, 4075–4094.

Limpasuvan, V., D. W. Thompson, and D. L. Hartmann, 2004: The life cycle of the Northern Hemisphere sudden stratospheric warmings. *Journal of Climate*, **17 (13)**, 2584–2596.

Marinaro, A., S. Hilberg, D. Changnon, and J. R. Angel, 2015: The North Pacific–driven severe midwest winter of 2013/14. *Journal of Applied Meteorology and Climatology*, **54 (10)**, 2141–2151.

Matsuno, T., 1970: Vertical propagation of stationary planetary waves in the winter Northern Hemisphere. *Journal of the Atmospheric Sciences*, **27 (6)**, 871–883.

Matsuno, T., 1971: A dynamical model of the stratospheric sudden warming. *Journal of the Atmospheric Sciences*, **28 (8)**, 1479–1494.

McIntyre, M. and T. Palmer, 1984: The 'surf zone'in the stratosphere. *Journal of Atmospheric and Terrestrial Physics*, **46 (9)**, 825–849.

National Academies of Sciences, Engineering and Medicine, 2016: Next generation earth system prediction: Strategies for subseasonal to seasonal forecasts. Tech. rep., National Academies of Sciences, Engineering and Medicine, Washington, DC. doi:10.17226/21873.

NOAA National Centres for Environmental Information, 2020: U.S. Billion-Dollar Weather and Climate Disasters. Accessed: 2020-06-10, `https://www.ncdc.noaa.gov/billions/`, accessed: 2020-06-10.

Peings, Y., 2019: Ural blocking as a driver of early-winter stratospheric warmings. *Geophysical Research Letters*, **46 (10)**, 5460–5468.

Plumb, R. A., 1985: On the three-dimensional propagation of stationary waves. *Journal of the Atmospheric Sciences*, **42 (3)**, 217–229.

Polvani, L. M. and D. W. Waugh, 2004: Upward wave activity flux as a precursor to extreme stratospheric events and subsequent anomalous surface weather regimes. *Journal of Climate*, **17 (18)**, 3548–3554.

Rao, J., C. I. Garfinkel, and I. P. White, 2020: Predicting the downward and surface influence of the February 2018 and January 2019 sudden stratospheric warming events in subseasonal to seasonal (s2s) models. *Journal of Geophysical Research: Atmospheres*, **125 (2)**, e2019JD031 919.

Robertson, A. W., A. Kumar, M. Peña, and F. Vitart, 2015: Improving and promoting subseasonal to seasonal prediction. *Bulletin of the American Meteorological Society*, **96 (3)**, ES49–ES53, doi:10.1175/BAMS-D-14-00139.1.

Scott, R., D. Dritschel, L. M. Polvani, and D. Waugh, 2004: Enhancement of Rossby wave breaking by steep potential vorticity gradients in the winter stratosphere. *Journal of the Atmospheric Sciences*, **61 (8)**, 904–918.

Smith, K. L., L. M. Polvani, and L. B. Tremblay, 2018: The impact of stratospheric circulation extremes on minimum Arctic sea ice extent. *Journal of Climate*, **31 (18)**, 7169–7183.

Thompson, D. W. and J. M. Wallace, 2000: Annular modes in the extratropical circulation. part i: Month-to-month variability. *Journal of Climate*, **13 (5)**, 1000–1016.

Thompson, D. W. and J. M. Wallace, 2001: Regional climate impacts of the Northern Hemisphere annular mode. *Science*, **293 (5527)**, 85–89.

Tibaldi, S. and F. Molteni, 1990: On the operational predictability of blocking. *Tellus A*, **42 (3)**, 343–365.

Tseng, K.-C., E. Barnes, and E. Maloney, 2018: Prediction of the midlatitude response to strong Madden-Julian Oscillation events on s2s time scales. *Geophysical Research Letters*, **45 (1)**, 463–470.

Vitart, F. and A. W. Robertson, 2018: The Sub-Seasonal to Seasonal Prediction Project (S2S) and the prediction of extreme events. *NPJ Climate and Atmospheric Science*, **1**.

Vitart, F., et al., 2017: The Subseasonal to Seasonal (S2S) Prediction Project Database. *Bulletin of the American Meteorological Society*, **98 (1)**, 163–173, doi: 10.1175/BAMS-D-16-0017.1.

White, C., S. Franks, and D. McEvoy, 2015: Using subseasonal-to-seasonal (S2S) extreme rainfall forecasts for extended-range flood prediction in Australia. *IAHS-AISH Proceedings and Reports*, **370**, 229–234.

Zhang, P., Y. Wu, I. R. Simpson, K. L. Smith, X. Zhang, B. De, and P. Callaghan, 2018: A stratospheric pathway linking a colder siberia to Barents-Kara Sea sea ice loss. *Science Advances*, **4 (7)**, eaat6025.